J Physiol Sci (2016) 66:15–41
DOI 10.1007/s12576-015-0412-5

REVIEW

Open-loop static and dynamic characteristics of the arterial baroreflex system in rabbits and rats

Toru Kawada[1] · **Masaru Sugimachi**[1]

Received: 28 September 2015 / Accepted: 30 September 2015 / Published online: 5 November 2015

Abstract The arterial baroreflex system is the most important negative feedback system for stabilizing arterial pressure (AP). This system serves as a key link between the autonomic nervous system and the cardiovascular system, and is thus essential for understanding the pathophysiology of cardiovascular diseases and accompanying autonomic abnormalities. This article focuses on an open-loop systems analysis using a baroreceptor isolation preparation to identify the characteristics of two principal subsystems of the arterial baroreflex system, namely, the neural arc from pressure input to efferent sympathetic nerve activity (SNA) and the peripheral arc from SNA to AP. Studies on the static and dynamic characteristics of the two arcs under normal physiological conditions and also under various interventions including diseased conditions are to be reviewed. Quantitative understanding of the arterial baroreflex function under diseased conditions would help develop new treatment strategies such as electrical activation of the carotid sinus baroreflex for drug-resistant hypertension.

Keywords Arterial pressure · Sympathetic nerve activity · Systems analysis · Equilibrium diagram · White noise · Transfer function

Introduction

The arterial baroreflex system is one of the most important negative feedback systems for stabilizing arterial pressure (AP) during daily activities. This system represents a typical example of homeostasis: a certain physiological variable is controlled within a small normal range against exogenous disturbances or environmental changes. A review by Sagawa [1] in the Handbook of Physiology covers a wide range of research results on the arterial baroreflex system, and it might appear that there is nothing more to add. Nevertheless, the present article tries to address more recent topics related to open-loop static and dynamic characteristics of the arterial baroreflex system in rabbits and rats, with an emphasis on analytical methods. As for the open-loop static characteristics, studies using a baroreflex equilibrium diagram analysis are reviewed. The baroreflex equilibrium diagram schematically describes how the operating point of the arterial baroreflex is determined through an interaction between the autonomic nervous system and the cardiovascular system [2, 3]. As for the open-loop dynamic characteristics, studies using a frequency-domain transfer function analysis based on a white noise approach are reviewed. White noise analysis, developed in the engineering field, is a powerful analytical method for identifying dynamic characteristics of a system even in the presence of significant noise contamination [4, 5]. Identification of the dynamic characteristics helps understand the quickness and stability of the arterial baroreflex system in regulating AP.

Pathways

Details about the central and peripheral pathways of the arterial baroreflex system can be found, for instance, in a review by Kumada et al. [6]. Briefly, changes in AP are

✉ Toru Kawada
torukawa@ncvc.go.jp

[1] Department of Cardiovascular Dynamics, National Cerebral and Cardiovascular Center, 5-7-1 Fujishirodai, Suita, Osaka 565-8565, Japan

sensed by arterial baroreceptors located at the areas of the carotid bifurcation (the bifurcation of the common carotid artery into the internal and external carotid arteries) and the aortic arch. When AP is elevated, the arterial wall is stretched, and baroreceptor afferent fibers discharge via opening of stretch-activated ion channels. The afferent signals from baroreceptors are transmitted to the nucleus tractus solitarius (NTS), from which second-order neurons project to the caudal ventrolateral medulla (CVLM). The CVLM sends inhibitory signals to the rostral ventrolateral medulla (RVLM) via GABAergic neurons. The inhibition of sympathetic outflow from the RVLM decreases AP via suppression of cardiac function and dilatation of resistance and capacitance vessels [7]. At the same time, other groups of neurons project from the NTS to the nucleus ambiguus [8] and the dorsal motor nucleus of vagus [9, 10]. Excitation of these nuclei increases vagal nerve activity, contributing to a decrease in heart rate (HR). When AP decreases, the opposite responses occur to restore AP toward the baseline level; but how is the baseline level of AP determined? This topic is discussed later in the section entitled "Baroreflex equilibrium diagram and operating point."

History

The discovery of the arterial baroreflex system is described in detail, for instance, in a book chapter written by Persson [11]. Briefly, the aortic depressor nerve, which runs through the neck region, was first identified in rabbits by Ludwig and Cyon in 1866 [12, 13]. Afferent stimulation of the cut end of this nerve yielded depressor and bradycardic responses. At the time of discovery, whether the nerve endings were restricted to the aortic arch area or if they also extended to the heart was a matter of controversy. The current view is that the aortic depressor nerve originates from the aortic arch area, where the aortic baroreceptors reside. The aortic depressor nerve joins the vagal nerve during its course to the NTS. The cell bodies of the aortic depressor nerve are primarily found in the inferior ganglion (the nodose ganglion) of the vagal nerve [14].

The identification of the carotid sinus nerve (Hering's nerve) was approximately 60 years after that of the aortic depressor nerve. While the dilatation at the carotid bifurcation had been known as the "carotid sinus," its physiological significance had not been clarified. Czermak noted that pressure around his right upper neck brought about slowing of HR, and speculated that the swelling at the carotid sinus mechanically stimulated efferent vagal nerve to produce bradycardia ("Vagusdruckversuch") [12]. Doubt was cast by Hering about the above interpretation. He performed a series of studies from 1923 to 1927 to demonstrate that the bradycardia was caused by a reflex arising from the carotid sinus [15]. The carotid sinus nerve joins the glossopharyngeal nerve and projects to the NTS. The cell bodies of the carotid sinus nerve are mainly found in the superior ganglion and inferior ganglion (the petrosal ganglion) of the glossopharyngeal nerve [16].

Open-loop analysis and other methods for estimating arterial baroreflex function

Two principal subsystems of arterial baroreflex system

The arterial baroreflex system serves as a key link between the autonomic nervous system and the cardiovascular system. The sympathetic limb of the arterial baroreflex system may be divided into two principal subsystems [17]. One is the "neural arc" subsystem, which determines sympathetic nerve activity (SNA) in response to a baroreceptor pressure input. The other is the "peripheral arc" subsystem, which determines AP as a result of the cardiovascular response to SNA. A cascade combination of the neural and peripheral arcs, which is referred to hereafter in this article as "total reflex arc," determines the AP output in response to the baroreceptor pressure input. From the viewpoint of control theory, the neural arc acts as a controller and the peripheral arc as a plant (or a controlled element) in a negative feedback system. Under normal physiological conditions, changes in AP affect SNA through the neural arc, whereas changes in SNA, in turn, affect AP through the peripheral arc. This closed-loop negative feedback operation gives rise to a chicken-and-egg problem between SNA and AP. An observational study where SNA and AP are measured under baroreflex closed-loop conditions does not usually allow separate identification of the input–output relationships of the neural and peripheral arcs.

Carotid sinus isolation

When baroreceptor regions are vascularly isolated from the systemic circulation, changes in AP no longer affect the baroreceptor input pressure, i.e., the baroreflex negative feedback loop is opened. Following a study by Moissejeff [18], carotid sinus isolation may be the most widely used method for opening the baroreflex negative feedback loop. The internal, external, and common carotid arteries are occluded, and the pressure in the carotid sinus region is externally controlled. The Moissejeff procedure and its modifications have been used for studies in anesthetized dogs [19–23], rabbits [17, 24–27], and rats [28–31]. A reversible isolation is also possible, which has been

reported for studies under conscious conditions in dogs [32–35] and rats [36].

By using the carotid sinus isolation procedure, open-loop characteristics of the neural and peripheral arcs can be examined over an entire input pressure range and also over a wide frequency range of physiological interest. A major disadvantage of the carotid sinus isolation is that it cannot be applied in human studies. Another disadvantage is that the aortic depressor and vagal nerves need to be sectioned to avoid confounding reflex effects from the aortic arch and cardiopulmonary regions. As a result, the contribution of the vagal limb to the baroreflex-mediated AP control cannot be evaluated. Regarding this limitation, studies examining the effects of afferent [37] or efferent [38] vagal nerve stimulation on the open-loop characteristics of the carotid sinus baroreflex may provide clues to understand the role of the vagal limb in the baroreflex-mediated AP control.

Aortic baroreceptor isolation

While a bypass operation on the aortic arch is required to isolate the receptor areas of the aortic depressor nerves bilaterally [39], the receptor area of the right aortic depressor nerve can be isolated around the bifurcation of the brachiocephalic artery into the right common carotid and subclavian arteries without the bypass operation [30, 40, 41]. To establish open-loop conditions for the aortic baroreflex, the carotid sinus and vagal nerves may need to be sectioned. The necessity of vagotomy is a common drawback in the carotid sinus and brachiocephalic isolation procedures.

The aortic depressor nerve is, in most occasions, separable from the vagal and cervical sympathetic nerves as a thin bundle in rabbits and rats. This anatomical feature enables manipulation of the aortic depressor nerve. For instance, periaxonal application of a pharmacological agent can be used to block the conduction of unmyelinated C-fibers in the aortic depressor nerve [42]. Another merit of the brachiocephalic isolation is that the aortic depressor nerve chiefly consists of baroreceptor afferent fibers, and baroreflex responses can be observed with minimal contamination by chemoreflex responses [43]. A demerit of the brachiocephalic isolation is that the reflex response is smaller than that can be obtained by using the bilateral carotid sinus isolation procedure.

Pharmacological arterial pressure perturbation

A pharmacological AP perturbation, such as that using intravenous phenylephrine and sodium nitroprusside administrations, is widely used to assess arterial baroreflex function. This method does not require baroreceptor isolation and can be applied in human studies. Nevertheless, it cannot replace open-loop analysis using baroreceptor isolation because of the following reasons. First, the arterial baroreflex-mediated AP response cannot be measured independently of the test drug-induced AP change. Hence, it is impossible to evaluate the arterial baroreflex control of AP. Second, vasoactive test drugs can modify the mechanical properties of the arterial wall around the baroreceptors, and the observed response may not be the same as that induced by a pure pressure input [44]. Third, it is difficult to precisely control the range and ramp speed of the AP perturbation, which can cause an estimation error of arterial baroreflex function. A rapid AP change can augment the SNA response due to the dynamic characteristics of the baroreflex neural arc [45].

Neck suction

Neck suction is a method of applying negative pressure around the neck to elicit responses from the carotid sinus baroreflex [46]. Although this method offers a unique opportunity to observe the baroreflex-mediated AP response in humans, it has its own limitations. First, transmural pressure at the carotid sinus region is not exactly assessed due to the presence of tissues between the skin and the carotid sinus. Although Ludbrook et al. [47] measured tissue pressure near the carotid sinus region invasively, such a measurement may not be routinely feasible. Second, the transmural pressure changes with AP even if the applied negative pressure is constant, which needs to be taken into account during the assessment of arterial baroreflex function. Third, the aortic baroreflex can counteract the carotid sinus baroreflex and attenuate the AP response [48]. To avoid influences from reflexes other than the carotid sinus baroreflex, an assessment of the initial HR response before any counteraction takes place has been previously proposed. However, the initial HR response may not fully reflect the sympathetic control of HR because the sympathetic control of HR is slower than the vagal control of HR [49, 50]. Likewise, the baroreflex-mediated sympathetic control of AP may not reach steady state within a time frame of the initial HR response. As a result, neck suction also does not allow an accurate assessment of the ability of the arterial baroreflex to regulate AP.

Mild and quick hemorrhage

Hosomi [51] developed a method of mild and quick hemorrhage to estimate open-loop gain, G, under baroreflex closed-loop conditions. The idea stems from the fact that an external disturbance, D, imposed on a negative feedback system will eventually be attenuated to $D' = D/(1 + G)$ when the system is stable. The size of D is assessed from

the AP drop immediately after hemorrhage and before the negative feedback buffering begins to occur. The size of *D*' is assessed from the steady-state AP fall. A potential weakness of this method is that accurate assessments of *D* and *D*' are not so easy due to the development of a pressure gradient across the circulatory system during the quick hemorrhage. AP restoration after the hemorrhage may be partly attributable to redistribution of blood. As an alternative method, *D* is assessed from the steady-state AP fall induced by an identical hemorrhage after all reflex systems are disabled by denervation [52]. However, disabling reflex systems can change the baseline level of AP and introduce further estimation error because baroreflex gain depends on the operating point due to the nonlinearity of the system.

Pressure pulse

Suga and Ohsima [53] reported another closed-loop identification method using a pressure pulse to estimate the transfer function of the carotid sinus baroreflex. The pressure pulse was added from a side arm of a T-shaped tube inserted in the middle of the common carotid artery. The pressure pulse was approximated by a Dirac delta function, and the AP response was assumed to be a damped sine wave function. The transfer function of the carotid sinus baroreflex was estimated by using the Laplace transform. While it was not mentioned, the aortic baroreflex, if not disabled, can counteract the carotid sinus baroreflex and modify the estimated transfer function. Note that an ideal impulse input, which has the infinite amplitude only at time zero with unity integral over time, is unrealizable. The deviation of the pressure pulse from the ideal impulse input could cause an estimation error of the transfer function unless the pressure pulse is treated otherwise. Another weakness of the pressure pulse method is that it may be susceptible to measurement noises such as unintentional AP variations frequently encountered in physiological experiments.

Static characteristics of arterial baroreflex system

Estimation of static characteristics

There may be no true steady state in biological systems in the sense that all living organisms are born, grow, and die. For convenience reasons, however, the response of a given system is assumed to reach steady state when time-dependent changes of the response become reasonably small. When a constant input pressure is imposed on the arterial baroreceptors, reflex changes occur in SNA and AP, and after a certain amount of time, the responses will settle at a new steady state. Static characteristics describe a set of steady-state responses measured over a wide input range of baroreceptor pressure. On the other hand, dynamic characteristics quantify transient responses, i.e., the time courses of how SNA and AP reach their steady-state responses.

To estimate the static characteristics of the arterial baroreflex over an entire input range an open-loop analysis is required. In a typical protocol, carotid sinus pressure (CSP) is changed in a staircase-wise manner. The non-pulsatile nature of the staircase-wise input is sometimes criticized as unphysiological because the pulsatility of input pressures affects baroreflex function [54, 55]. Not controlling the pulsatility, however, such as in the case with the pharmacological AP perturbation, could be more problematic than the absence of pulsatility when comparing arterial baroreflex function between different conditions. If the amplitude and frequency of input pulsatility are different between conditions, it may be difficult to determine whether the observed difference is attributable to the change in the input pulsatility or an actual difference in baroreflex function.

The input–output relationship of the total reflex arc approximates an inverse sigmoid curve, therefore the input pressure range needs to be determined so that threshold and saturation can be observed. For instance, CSP is changed from 50 to 200 mmHg in increments of 25 mmHg [19, 20] or from 25 to 300 mmHg in increments of 25 mmHg [21] in studies on dogs. CSP is changed from 40 to 140 mmHg in increments of 10 mmHg [24] or from 40 to 160 mmHg in increments of 20 mmHg [56] in studies on rabbits. CSP is changed from 80 to 160 mmHg in increments of 10 mmHg and back from 160 to 80 mmHg in decrements of 10 mmHg [3] or from 60 to 180 mmHg in increments of 20 mmHg [31, 38] in rats because the operating range of the arterial baroreflex is slightly higher than in rabbits.

To allow the AP response to reach a new steady state, each CSP level of the staircase-wise input needs to be held for a sufficient amount of time. The step duration is somewhat empirically determined by investigators' expertise. In dogs, the step duration varies among studies, e.g., 15 s [57], 20 s [21], 90 s [20], and 60–120 s [19]. A step duration of 15 s might be a little short in dogs because data may need to be averaged for 5–10 s to obtain a steady-state response. In rabbits, 60-s step duration [56] may be sufficiently long to obtain the steady-state response [17]. In rats, the step duration has ranged from 20 [37] to 60 s [3, 31, 38]. In fact, a 20-s step duration provides an estimation of the open-loop static characteristics of the carotid sinus baroreflex that is comparable to a 60-s step duration in rats [58].

Static characteristics of the total reflex arc

Static characteristics of the total reflex arc, determined as the steady-state input–output relationship between CSP and AP, approximate an inverse sigmoid curve and can be quantified by a four-parameter logistic function as follows [59]:

$$y = \frac{P_1}{1 + \exp[P_2(x - P_3)]} + P_4 \quad (1)$$

where x and y indicate the input and output, respectively; P_1 is the response range or the difference between the maximum and minimum values of y; P_2 is the slope coefficient; P_3 is the midpoint of the sigmoid curve on the x axis; and P_4 is the minimum value of y.

The first derivative of the four-parameter logistic function provides a gain curve function as follows:

$$y' = -\frac{P_1 P_2 \exp[P_2(x - P_3)]}{\{1 + \exp[P_2(x - P_3)]\}^2} \quad (2)$$

This gain curve function gives the (negative) maximum gain of $-P_1P_2/4$ at $x = P_3$. Considering the negative feedback operation of the arterial baroreflex system, the negative sign is usually omitted in describing the gain values. The threshold and saturation points on the x axis are calculated as follows:

$$x = P_3 \pm \frac{k}{P_2} \quad (3)$$

The width of the input range, i.e., the difference between the saturation and threshold points on the x axis, is given by $2k/P_2$. Kent et al. [59] suggested using $k = 1.317$, but this value has been argued to be too small to represent the threshold and saturation points by other investigators. If 95 % and 5 % of the response range on the y axis are first specified to calculate the threshold and saturation points on the x axis, respectively, k becomes 2.944 [60].

Shown in Fig. 1a is an example of the static characteristics of the total reflex arc estimated in Sprague–Dawley rats in our laboratory ($n = 12$, mean ± SE). The smooth curve indicates the four-parameter logistic function fitted to the 7 mean data points. The parameters are $P_1 = 74.4$ mmHg, $P_2 = 0.091$ mmHg^{-1}, $P_3 = 127.7$ mmHg, and $P_4 = 65.1$ mmHg, with r^2 of 0.999 between measured and fitted values. Figure 1b represents the gain curve function derived from the fitted logistic function. The maximum gain is calculated to be 1.70.

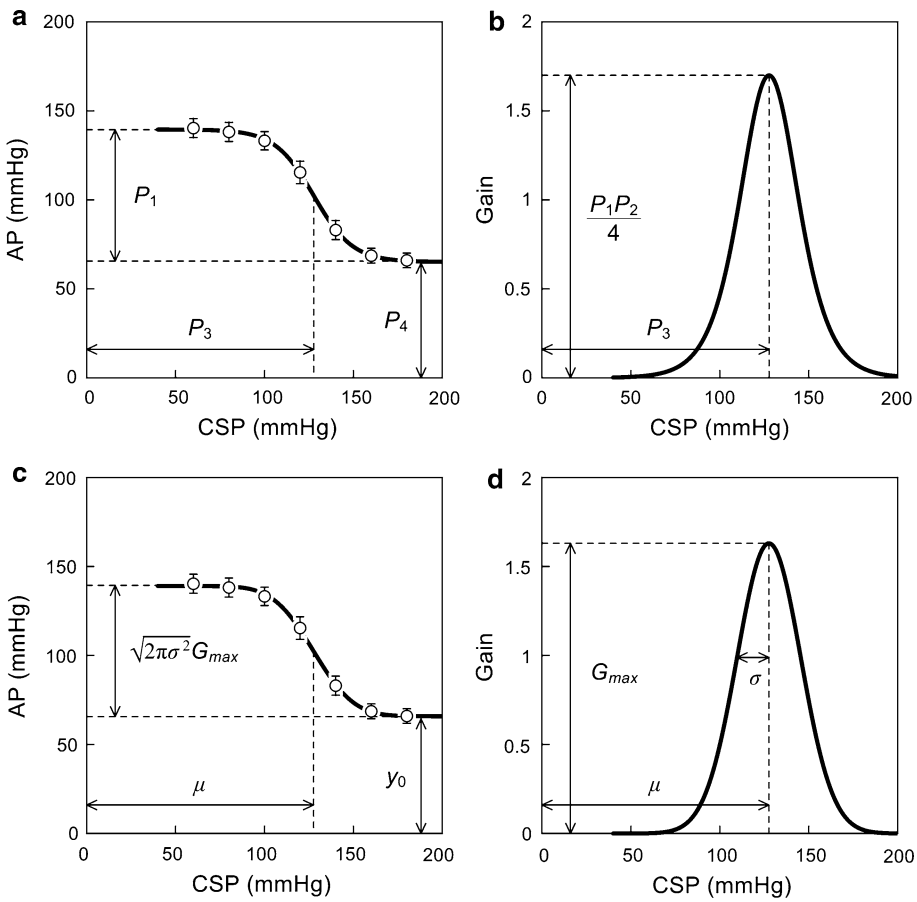

Fig. 1 Example of static characteristics of the total reflex arc from carotid sinus pressure (*CSP*) to arterial pressure (*AP*) obtained in Sprague–Dawley rats. **a** Quantification using a four-parameter logistic function. **b** Gain curve obtained from the first derivative of the fitted logistic function. **c** Quantification using an integral of a bell-shaped gain curve function. **d** Bell-shaped gain curve function corresponding to panel **c**. P_1 response range, P_2 slope coefficient, P_3 midpoint input pressure, P_4 minimum response. G_{max} maximum gain, σ standard deviation, μ midpoint input pressure, y_0 minimum response. In panels **a** and **c**, data points represent mean ± SE values ($n = 12$)

To describe the possible asymmetry of the measured CSP–AP curve, a fifth parameter may be added to the four-parameter logistic function [35, 61]. However, the addition of the fifth parameter makes the interpretation of each parameter more difficult (e.g., the input pressure that gives the steepest point of the sigmoid curve is no longer determined by P_3 alone). The four-parameter logistic function may be a practical compromise between the degrees of freedom for fitting and ease of interpretation of estimated parameters.

Another way to quantify the baroreflex static characteristics is to use a bell-shaped gain curve function similar to a normal distribution curve as follows [1, 24, 62]:

$$g = G_{\max}\exp\left[-\frac{(x-\mu)^2}{2\sigma^2}\right] \tag{4}$$

where x and g indicate the input and gain values, respectively; $G_{\max}$ is the maximum gain; μ is the midpoint on the x axis; and σ is the value corresponding to a standard deviation of the normal distribution curve. Integrating the bell-shaped gain curve function from $-\infty$ to x yields a sigmoidal input–output curve. Unfortunately, the solution cannot be expressed by a set of elementary functions. If the cumulative distribution function of a normal distribution, normdist(x), is computationally available, the following equation may be used to estimate the parameters by directly fitting the function to the measured input–output data:

$$y = \sqrt{2\pi\sigma^2}G_{\max}\left[1 - \text{normdist}\left(\frac{x-\mu}{\sigma}\right)\right] + y_0 \tag{5}$$

where y_0 represents the minimum value of y. Comparing with Eq. 1, μ corresponds to P_3, y_0 corresponds to P_4, and $\sqrt{2\pi\sigma^2}G_{\max}$ gives a value corresponding to P_1.

In Fig. 1c, the smooth curve represents the integral of the bell-shaped gain curve function fitted to the same 7 mean data points as Fig. 1a. The parameters are $G_{\max} = 1.63$, $\sigma = 17.9$ mmHg, $\mu = 127.6$ mmHg, and $y_0 = 65.9$ mmHg, with r^2 of 0.999 between measured and fitted values. The response range is calculated to be 73.2 mmHg. Shown in Fig. 1d is the corresponding bell-shaped gain curve function.

Although the four-parameter logistic function and the integral of the bell-shaped gain curve function do not match exactly, the r^2 value between the measured and fitted values is close to unity for both representations. Considering the limited number of data points and the presence of measurement errors in physiological experiments, both representations may be a reasonable approximation of the open-loop static characteristics of baroreflex function [63].

Static characteristics of the neural arc

Static characteristics of the neural arc, determined as the steady-state input–output relationship between CSP and SNA, can also be quantified using the four-parameter logistic function (Eq. 1) or the integral of the bell-shaped gain curve function (Eq. 5). A potential issue in describing the neural arc is the quantification of SNA. Although multifiber SNA is recorded in μV units, the absolute amplitude of SNA can vary considerably among animals depending on recording conditions such as the physical contact between the nerve and electrodes. One way to express SNA is to assign minimum and maximum SNA values during the staircase-wise CSP input to 0 and 100 %, respectively [3, 64, 65]. For the definition of 0 %, the noise level of SNA recorded after the intravenous administration of a ganglionic blocker hexamethonium bromide can also be used when SNA has been recorded from a postganglionic sympathetic nerve [31, 38]. In the hexamethonium method, the minimum SNA represents the magnitude of baroreflex-independent SNA. For the definition of 100 %, the baseline SNA at the closed-loop operating point can also be used [66]. The normalization of SNA helps compare SNA before and after a given intervention in an acute experimental setting. The comparison of SNA among different groups of animals is still a matter of concern because the normalization procedure can mask potential differences in the absolute SNA [67–69].

Shown in Fig. 2a is an example of the static characteristics of the neural arc estimated from the same rats as in Fig. 1. SNA is normalized such that the SNA at the CSP level of 60 mmHg becomes 100 % and the noise level measured after the ganglionic blockade becomes 0 % in each rat. The smooth curve indicates the four-parameter logistic function fitted to the 7 mean data points. The parameters are $P_1 = 64.6$ %, $P_2 = 0.085$ mmHg^{-1}, $P_3 = 132.1$ mmHg, and $P_4 = 35.2$ %, with r^2 of 0.999 between measured and fitted values.

Static characteristics of the peripheral arc

Static characteristics of the peripheral arc, determined as the steady-state input–output relationship between SNA and AP, can be described using a four-parameter logistic function [3, 66]. However, because the peripheral arc is approximately linear in the range of normal baroreflex control [31, 38], it can also be quantified using a regression line as follows:

$$y = b_0 + b_1 x \tag{6}$$

where b_0 and b_1 are the intercept and slope, respectively.

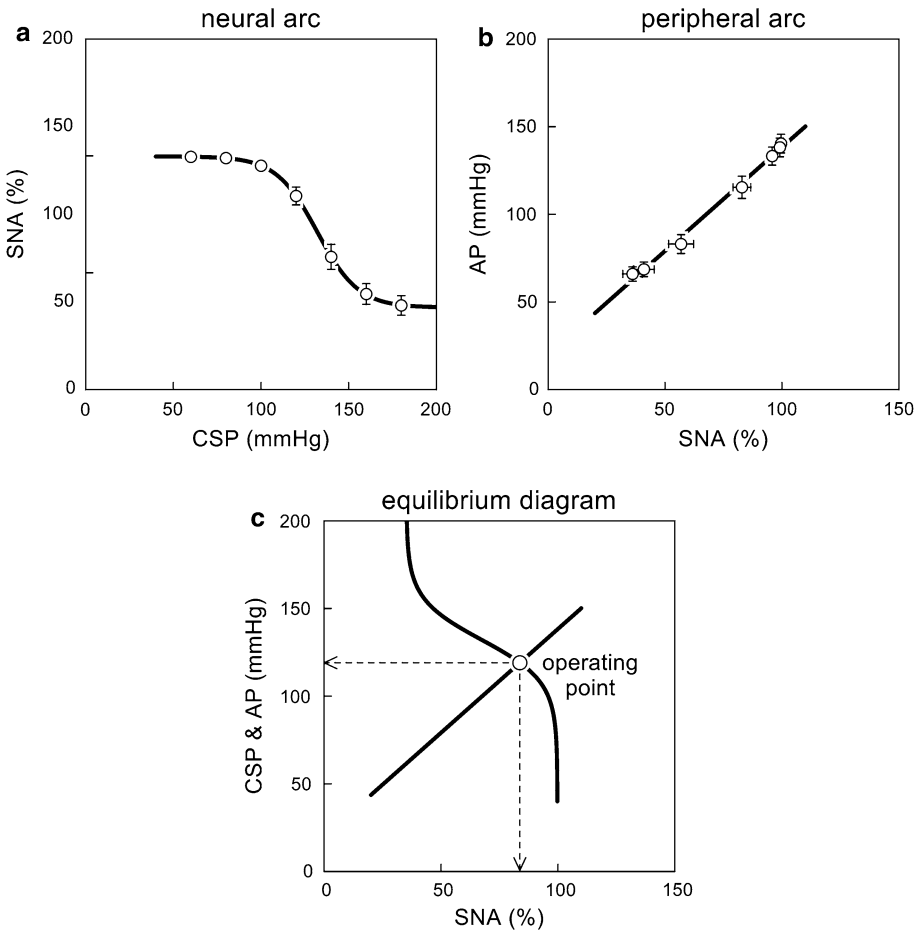

Fig. 2 **a** Example of static characteristics of the neural arc from carotid sinus pressure (*CSP*) to sympathetic nerve activity (*SNA*). The *smooth curve* indicates a four-parameter logistic function fitted to the mean data points. **b** Example of static characteristics of the peripheral arc from *SNA* to arterial pressure (*AP*). The *straight line* indicates a regression line over the mean data points. **c** Baroreflex equilibrium diagram drawn from the fitted neural arc and peripheral arc. The intersection between the two arcs yields an operating point, which is the point of operation when the baroreflex negative feedback is closed. In panels **a** and **b**, data are mean ± SE values ($n = 12$) derived from the same Sprague–Dawley rats as in Fig. 1

Shown in Fig. 2b is an example of the static characteristics of the peripheral arc estimated from the same rats as Fig. 1. The oblique line illustrates the regression line fitted to the 7 mean data points. The parameters are $b_0 = 20.0$ mmHg and $b_1 = 1.18$ %/mmHg, with r^2 of 0.994.

Baroreflex equilibrium diagram and operating point

An operating point is a point that AP settles at under baroreflex closed-loop conditions. The intersection between the CSP–AP curve and the line of identity gives the operating point [1], because CSP is the same as AP when the baroreflex negative feedback loop is closed. (Strictly speaking, pressure waveforms may be different between CSP and AP and hydrostatic pressure may develop depending on posture. These effects, however, are ignored here to simplify the discussion on the operating principle of the arterial baroreflex system.) The operating point is sometimes regarded as a set point as if it is a predefined target level of the AP control. In reality, however, the operating point may be determined from an interaction between the autonomic nervous system and the cardiovascular system as discussed below.

When open-loop static characteristics are identified for both the neural and peripheral arcs, the two can be plotted on a pressure–SNA plane as shown in Fig. 2c. The intersection between the two arcs provides the closed-loop operating point. The concept of "baroreflex equilibrium diagram" or "baroreflex balance diagram" is found in a book entitled Cardiovascular Physiology written by Mohrman and Heller [2]. A study by Sato et al. [3] may have been the first to experimentally validate the utility of the baroreflex equilibrium diagram in anesthetized rats. In that study, hemorrhage did not significantly affect the neural arc but changed the peripheral arc, which explains an increase in SNA and a decrease in AP during hemorrhage. Furthermore, the operating-point SNA and AP predicted from the baroreflex equilibrium diagram were close to those actually measured under baroreflex closed-loop conditions. The utility of the baroreflex equilibrium diagram under a variety of pathophysiological conditions is further reviewed in the

section entitled "Effects of various interventions on open-loop baroreflex characteristics."

When the neural and peripheral arcs are modeled by a four-parameter logistic function and a regression line, respectively, the operating point (an intersection of the two arcs) is determined computationally by using a binary search algorithm. A product of the tangential slope of the neural arc and the slope of the peripheral arc at the operating point gives the total reflex gain at the operating point [70].

Static characteristics of baroreceptor transduction and central processing

The neural arc can be further divided into a subsystem of baroreceptor transduction and a subsystem of central processing from baroreceptor afferent nerve activity to efferent SNA. The characteristics of the mechano–neural transduction from pressure input to afferent nerve activity can be quantified using the four-parameter logistic function (Eq. 1) for both the carotid sinus [71, 72] and aortic baroreceptors [41]. The slope coefficient, P_2, is calculated to be a negative value because afferent nerve activity increases as the input pressure increases.

With respect to the carotid sinus baroreflex in rabbits, the midpoint pressure, P_3, is lower (89.9 ± 3.4 mmHg [72] vs. 114.6 ± 11.9 mmHg [73]) and the absolute value of P_2 is smaller (0.072 ± 0.010 $mmHg^{-1}$ [72] vs. 0.110 ± 0.028 $mmHg^{-1}$ [73]) in the baroreceptor transduction than in the neural arc. Similarly, with respect to the aortic baroreflex in rats, P_3 is lower (118 ± 4 mmHg [41] vs. 129.1 ± 4.5 mmHg [42]) and the absolute value of P_2 is smaller (0.088 ± 0.009 $mmHg^{-1}$ [41] vs. 0.146 ± 0.016 $mmHg^{-1}$ [42]) in the baroreceptor transduction than in the neural arc. These results indicate the presence of significant nonlinearity in the central processing from baroreceptor afferent nerve activity to efferent SNA.

The relationship between electrical stimulation of the carotid sinus nerve and renal SNA reveals an intensity-dependent suppression with saturation nonlinearity at high intensities in dogs [21]. Interestingly, in a study by Hosokawa et al. [74], a bionic baroreceptor system reproduced the sigmoidal AP response to pressure input to a reasonable extent in anesthetized rats. An offset pressure to activate the bionic baroreceptor system was introduced but otherwise the system operated linearly. Therefore, the saturation of the AP response might have been attributable to the nonlinear relationship between the baroreceptor stimulation and AP. These results suggest that the mechano–neural transduction at the arterial baroreceptors alone does not determine the overall sigmoidal nonlinearity of the arterial baroreflex.

Dynamic characteristics of the arterial baroreflex system

Estimation of dynamic characteristics

Experimental protocol

To estimate dynamic characteristics of the arterial baroreflex, a transfer function analysis using a white noise input has been employed. White noise is rich in frequency components and is efficient for estimating dynamic characteristics of a biological system from a limited length of data. The theoretical background of transfer function analysis can be found in detail in a book written by Bendat and Piersol [5]. Another book written by Marmaleris and Marmaleris [4] covers a wide variety of topics about the application of white noise analysis to physiological systems. The following paragraphs focus on the practical application of white noise analysis to the arterial baroreflex system including experimental protocols.

When imposing a white noise input to CSP, the mean level is set near the operating-point AP, which can be determined in each animal by measuring AP in advance of isolating the carotid sinus regions [75] or by adjusting CSP to AP via a servo-controlled piston pump system [45, 56, 73, 76]. A fixed value may also be used based on the operating-point AP estimated from the open-loop static characteristics of the carotid sinus baroreflex. Using a fixed value is preferable when comparing dynamic characteristics between different groups because a possible effect of a difference in the operating point can be excluded. For instance, a mean of 120 mmHg was used to compare the dynamic characteristics between normal rats and rats with chronic heart failure [67].

The amplitude of the white noise input is selected to obtain SNA and AP responses large enough to estimate the transfer function. If the input amplitude is too small, estimation of the transfer function becomes inaccurate due to a low signal-to-noise ratio in the output measurement. Two types of white noise signals are mainly used: binary white noise and Gaussian white noise. Binary white noise alternates between two values. For example, CSP values of 10 [45] or 20 mmHg [56, 73, 75, 76] above and below the mean pressure have been used. It should be noted that the input amplitude of the binary white noise can affect the shape of the estimated transfer function [77]. Gaussian white noise has values with normal distribution around the mean. A Gaussian white noise signal with a mean of 120 mmHg and a standard deviation of 20 mmHg has been used to cover the input range of the carotid sinus baroreflex in normotensive rats [67]. Gaussian white noise has an advantage over binary white noise in that the nonlinearity

of a system does not affect the estimation of the linear transfer function except for a factor of proportionality if the system is described by a class of finite memory nonlinear systems [67, 78]. It also allows the extension of the analysis toward higher-order nonlinear dynamics of the system [4].

The switching interval of the white noise is selected to cover the upper bound of the frequency range of physiological interest. When the switching interval is set to 0.5 s (2 Hz), the input power spectral density is relatively flat up to 0.5 Hz, decreases to approximately 50 % at 1 Hz and approximately 10 % at 1.5 Hz, and diminishes as the frequency approaches 2 Hz [73]. A switching interval of 0.5 s may be sufficiently short to estimate the transfer function in rabbits because of the low-pass characteristics of the total reflex arc [17]. In rats, the switching interval may be shortened to 0.4 s in order to identify the transfer function up to slightly higher frequencies [45]. When the dynamic characteristics of the neural arc in the higher frequency range are of particular interest, the switching interval can be reduced to 0.05 s (20 Hz) [79].

The required data length is related to a segment length (T_s) and the number of segments (N_s) in the data analysis described in the next section. If the segments are taken in a half-overlapping manner, the minimum data length is $T_s(N_s + 1)/2$. Some additional length is needed, however, because data from initial few minutes after the initiation of the white noise input may need to be discarded to analyze only the stationary portion of the recorded data. N_s is typically selected to be between 8 and 12 for a stable estimation of the transfer function. The reciprocal of T_s gives the lower frequency bound (the fundamental frequency or the frequency resolution) of the Fourier analysis. T_s is typically set at 102.4 s [17, 45, 73], which corresponds to the lower frequency bound of $1/T_s = 0.0098$ Hz. When T_s is properly selected, the estimated transfer function does not show significant frequency-dependent changes of the dynamic gain near the lower frequency bound. In addition, the phase value approaches either zero or $-\pi$ radians at the lowest frequency, depending on whether the input–output relationship is positive or negative. If these conditions are not met, T_s may need to be prolonged together with an extension of the total data length.

Data analysis

In a typical data analysis, the input–output data pairs are resampled at 10 Hz, and divided into half-overlapping segments of 1024 points each. In each segment, a linear trend is removed and a Hanning window is applied. Thereafter, the frequency spectra of input, $X(f)$, and output, $Y(f)$, are calculated via the fast Fourier transform. In the discrete Fourier transform, f represents a zero-based index of the frequency, and the actual frequency is given by f/Ts (in Hz). Ensemble averages of the input power spectra, $S_{XX}(f)$, the output power spectra, $S_{YY}(f)$, and the cross spectra between the input and output, $S_{YX}(f)$, are calculated over the N_s segments. Finally, the transfer function from the input to output is estimated from the following equation [4, 5]:

$$H(f) = \frac{S_{YX}(f)}{S_{XX}(f)} \tag{7}$$

As the equation indicates, a sufficient input power is needed over the frequency of interest for the stable estimation of $H(f)$ because the lack of input power causes division by a small number at the corresponding frequencies. The white noise input fulfills the requirement for the sufficient input power over a wide frequency range. The transfer function is a complex-valued function and can be expressed by its modulus (gain) and phase at each frequency. The magnitude-squared coherence function is calculated as follows [4, 5]:

$$\mathrm{Coh}(f) = \frac{|S_{YX}(f)|^2}{S_{XX}(f)S_{YY}(f)} \tag{8}$$

The coherence function ranges from zero to unity, and represents the power ratio of the linearly predicted output to the measured output. The coherence decreases from unity when the output contains noise contamination, nonlinear system responses, or both.

After the transfer function in the frequency domain is identified, an impulse response of the system in the time domain, $h(\tau)$, can be obtained via the inverse Fourier transform. The system response to an arbitrary input is then calculated from a convolution as follows:

$$y(t) = \int_{-T_s/2}^{T_s/2} h(\tau)x(t-\tau)\mathrm{d}\tau \tag{9}$$

For a causal system, $h(\tau)$ is supposed to be zero for $\tau < 0$. As a special case of Eq. 9, a step response of the system, $s(t)$, is derived from a time integral of the impulse response as follows:

$$s(t) = \int_0^t h(\tau)\mathrm{d}\tau \tag{10}$$

Why should we bother to calculate the step response via the transfer function analysis? If the system is purely linear and the step response is measured under noiseless conditions, the measured step response will be the same as the step response derived from the transfer function. In the case of experiments in physiological systems, to a certain extent, the system will usually exhibit nonlinear responses. Furthermore, the output is contaminated with measurement noise and physiological variations unrelated to the input. Under these conditions, white noise analysis yields a robust

estimation of the linear dynamics of the system [4]. A slightly extended discussion of this topic is given in the section entitled "Closed-loop identification of open-loop dynamic characteristics."

Bode plot

The estimated dynamic transfer function may be expressed in the form of a Bode plot, which is comprised of gain and phase plots. The gain plot is a log–log plot where the logarithms of dynamic gain values are displayed against the logarithms of frequencies. The phase plot is a semi-log plot where phase values are displayed against the logarithms of frequencies.

The slope of the dynamic gain, in a certain frequency range, is sometimes used to describe the system dynamic characteristics. Several units are available to express the frequency-dependent changes in the dynamic gain. The terms "octave" and "decade" denote a twofold and a tenfold change in the frequency, respectively. A change in the dynamic gain value can be expressed in units of dB (decibel) using the following equation:

$$V_{\mathrm{dB}} = 20\log_{10}\left(\frac{G_{f2}}{G_{f1}}\right) \tag{11}$$

where V_{dB} is a value in dB units; and G_{f1} and G_{f2} denote dynamic gain values at two different frequencies, respectively. For instance, if the dynamic gain increases from 1 to 10 as the frequency increases tenfold, the slope of dynamic gain is 20 dB/decade. A conversion factor from dB/decade into dB/octave can be obtained by solving $2^x = 10$, which gives $x = 3.322$. Hence the slope of 20 dB/decade equals to $20/3.322 = 6.0$ dB/octave.

Dynamic characteristics of the neural arc

In a study by Ikeda et al. [17], the neural arc transfer function from CSP to SNA reveals high-pass or derivative characteristics in rabbits, which means that the dynamic gain of the neural arc increases as the input modulation frequency increases. The derivative characteristics are observed in the frequency range above approximately 0.1 Hz. Instead of enumerating the gain and phase values for all frequencies, the following mathematical model can be used to describe the estimated neural arc transfer function:

$$H_N(f) = -K\left(1 + \frac{f}{f_{\mathrm{C}}}j\right)\exp(-2\pi f\,Lj) \tag{12}$$

where f and j represent the frequency (in Hz) and the imaginary units, respectively; and K, f_C, and L represent the steady-state gain, corner frequency (in Hz), and pure delay (in s), respectively. The negative sign for K indicates a signal inversion through the neural arc, i.e., an increase in CSP decreases SNA at steady state. The transfer function value reaches $-K$ (i.e., the dynamic gain of K and phase of $-\pi$ radians) as the frequency approaches zero. On the other hand, the dynamic gain increases as the frequency increases beyond f_{C}. A tenfold increase in the frequency results in a tenfold increase in the dynamic gain when $f \gg f_{\mathrm{C}}$, i.e., the slope of dynamic gain is asymptotically 20 dB/decade.

In the above study by Ikeda et al. [17], the physiological significance of the derivative characteristics of the neural arc was examined using a numerical simulation. An advantage of the numerical simulation over an animal experiment is that it is possible to hypothetically alter key parameters of the system, even beyond their normal physiological ranges, and to examine what the results would become. Based on a simulation that removes or enhances the derivative characteristics, the neural arc was shown to compensate for the slow peripheral arc to accelerate the baroreflex control of AP [17].

If the derivative characteristics of the neural arc continue in the frequency range higher than 1 Hz, pulsatile pressure occurring at frequencies 3–5 Hz (180–300 beats/min) could saturate the central processing in rabbits. However, the saturation is avoided by virtue of the presence of high-cut characteristics in the frequency range above approximately 0.8 Hz [79]. To describe the high-cut characteristics of the neural arc, the following mathematical model can be used:

$$H_N(f) = \frac{-K\left(1 + \frac{f}{f_{\mathrm{C1}}}j\right)}{\left(1 + \frac{f}{f_{\mathrm{C2}}}j\right)^2}\exp(-2\pi f\,Lj) \tag{13}$$

where K, f_{C1}, f_{C2}, and L represent the steady-state gain, corner frequency relating to the derivative characteristics (in Hz), corner frequency relating to the high-cut characteristics (in Hz), and pure delay (in s), respectively. The dynamic gain increases in the frequency range above f_{C1} and decreases in the frequency range above f_{C2}, assuming $f_{\mathrm{C1}} < f_{\mathrm{C2}}$.

Figure 3a depicts an example of the neural arc transfer function estimated by using a Gaussian white noise input with a mean of 120 mmHg and a standard deviation of 20 mmHg from Sprague–Dawley rats in our laboratory ($n = 12$, mean ± SE, thin gray lines). The dynamic gain is normalized so that the average gain value below 0.03 Hz becomes unity in each animal. In the gain and phase plots, the dotted line indicates the mathematical model (Eq. 13) fitted to the mean of the estimated transfer function in the frequency range up to 1.5 Hz. The parameters of the model are $K = 0.96$, $f_{\mathrm{C1}} = 0.12$, $f_{\mathrm{C2}} = 1.01$, and $L = 0.09$.

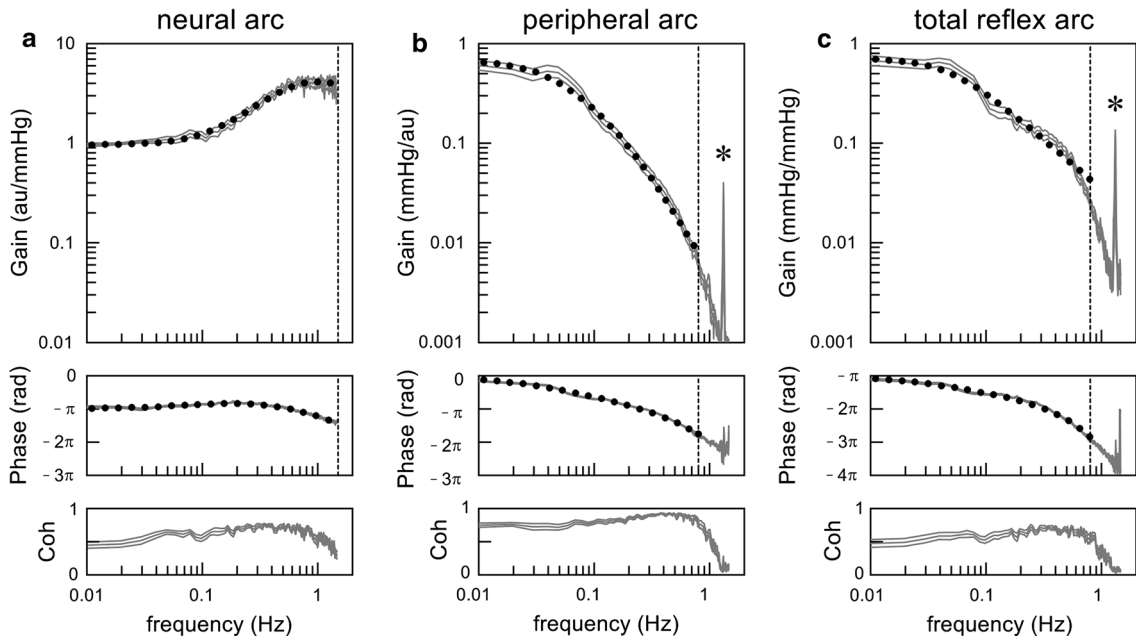

Fig. 3 Example of dynamic characteristics of the neural arc (**a**), peripheral arc (**b**), and total reflex arc (**c**) obtained in Sprague–Dawley rats. From *top to bottom*, the gain plot, phase plot, and coherence (Coh) plot are shown. The *gray lines* indicate estimated transfer functions shown up to 1.5 Hz (mean ± SE, $n = 12$). *Dotted curves* indicate mathematical models fitted to the mean of the transfer functions. The *vertical dotted lines* indicate the maximum frequency of fitting (1.5 Hz in the neural arc, and 0.8 Hz in the peripheral arc and total reflex arc). In the peripheral arc and total reflex arc transfer functions, a sharp peak is noted at 1.33 H, which is an artifact caused by mechanical ventilation (*asterisk*)

Dynamic characteristics of peripheral arc

The peripheral arc transfer function from SNA to AP shows low-pass characteristics, which means that the dynamic gain decreases with increasing frequency. The peripheral arc transfer function can be modeled by a second-order low-pass filter with pure delay as follows [17, 80]:

$$H_P(f) = \frac{K}{1 + 2\zeta\frac{f}{f_N}j + \left(\frac{f}{f_N}j\right)^2}\exp(-2\pi f\,Lj) \tag{14}$$

where K, f_N, ζ, and L represent the steady-state gain, natural frequency (in Hz), damping ratio (unitless), and pure delay (in s), respectively. The transfer function value reaches K (i.e., the dynamic gain of K and phase of zero radians) as the frequency approaches zero. The slope of dynamic gain in the frequency range above f_N asymptotically becomes −40 dB/decade. This model has also been used to describe the transfer function relating the sympathetic control of HR [50, 80–82] and the transfer function from electrical stimulation of the RVLM to AP [83].

In Fig. 3b, the thin gray lines indicate an example of the peripheral arc transfer function estimated from the same rats as in Fig. 3a. The dynamic gain of the peripheral arc is normalized by a reciprocal of the factor used for the neural arc in each animal so that the dynamic gain of the product of the neural and peripheral arcs is kept unchanged. A sharp peak at 1.33 Hz is an artifact caused by mechanical ventilation (80 cycles/min). In the gain and phase plots, the dotted line indicates the mathematical model (Eq. 14) fitted to the mean of the estimated transfer function in the frequency range up to 0.8 Hz. The parameters of the model are $K = 0.67$, $f_N = 0.088$, $\zeta = 1.36$, and $L = 0.53$.

Dynamic characteristics of the total reflex arc

Mathematically, a product of the model transfer functions of the neural arc (Eq. 13) and peripheral arc (Eq. 14) should provide a model transfer function of the total reflex arc, $H_T(f)$. Such a model, however, results in large variances in parameter estimation due to over-parameterization. Instead, $H_T(f)$ may be reduced to a first-order low-pass filter with pure delay as follows [17, 80]:

$$H_T(f) = -\frac{K}{1 + \frac{f}{f_C}j}\exp(-2\pi f\,Lj) \tag{15}$$

where K, f_C, and L represent the steady-state gain, corner frequency (in Hz), and pure delay (in s), respectively. The slope of dynamic gain in the frequency range above f_C asymptotically becomes −20 dB/decade. This model has also been used to describe the transfer function from vagal nerve stimulation to HR [50, 82, 84].

In Fig. 3c, the thin gray lines represent an example of the total reflex arc transfer function estimated from the same rats as in Fig. 3a. A sharp peak at 1.33 Hz is an artifact caused by mechanical ventilation. In the gain and phase plots, the dotted line indicates the mathematical model (Eq. 15) fitted to the mean of the estimated transfer function in the frequency range up to 0.8 Hz. The parameters of the model are $K = 0.71, f_C = 0.049$, and $L = 0.85$. Note that the estimated dynamic gain, K, is reduced depending on the input amplitude [67, 77], and is smaller than the maximum gain derived from the sigmoidal input–output relationship of the static characteristics of the total reflex arc.

While the mathematical model helps describe the estimated transfer function by a set of parameters instead of enumerating gain and phase values for all frequencies, the mathematical model is only an approximation and not a unique representation of the estimated transfer function. The first-order low-pass filter may be a little too simplistic to describe the total reflex arc transfer function. To describe the asymptotic decreasing slope of a dynamic gain steeper than –20 dB/decade [22] or to describe an oscillatory AP response [53], the second-order low-pass filter may be a better model for the transfer function of the total reflex arc. In an earlier study by Levison et al. [85], the total reflex arc transfer function is expressed as a more complex model including components of a second-order low-pass filter.

Dynamic characteristics of baroreceptor transduction and central processing

The transfer function of the neural arc can be subdivided into the transfer function representing the baroreceptor transduction and the transfer function from baroreceptor afferent nerve activity (or afferent nerve stimulation) to efferent SNA. The latter transfer function is referred to as "central arc" transfer function hereafter in this article. In a study by Kubo et al. [86], the dynamic gain of the central arc did not change significantly with changes in frequency in rabbits. However, the magnitude of derivative characteristics observed in the mechano–neural transduction at the aortic baroreceptors (approximately 6 dB/decade) [41] or at the carotid sinus baroreceptors (approximately 4.6 dB/decade) [72] is not large enough to fully explain the derivative characteristics observed in the neural arc transfer function (4.68 dB/octave = 15.5 dB/decade) [17], indicating that the central arc is likely to possess some derivative characteristics. This speculation is supported by the fact that the neural arc transfer function relating to cardiac SNA shows slightly enhanced derivative characteristics compared with that relating to renal SNA [73]. If the central arc does not modify the relative amplitude of the signals from baroreceptor afferents but only provides a fixed time delay, the magnitude of derivative characteristics would likely have been the same for both cardiac and renal SNAs. It may be of note that the transfer function of the neural arc does not significantly differ between cardiac and renal SNAs in cats [87]. Differences in species and experimental protocols may contribute to the inconsistent conclusions [73].

The diversity in the derivative characteristics of the central arc observed among various reports may be partly explained by the presence of two types of baroreceptor afferent fibers (i.e., myelinated A-fiber and unmyelinated C-fiber [88]) and the differences in stimulation protocols. When myelinated A-fiber afferent fibers are preferentially activated by low-voltage and high-frequency stimulation, the derivative characteristics of the central arc are more pronounced [89]. In contrast, when unmyelinated C-fiber afferent fibers are preferentially activated by high-voltage and low-frequency stimulation, the derivative characteristics of the central arc become attenuated.

Synaptic transmission requires a number of processes including changes in presynaptic membrane potentials, neurotransmitter release from the presynaptic nerve endings, neurotransmitter diffusion across the synaptic clefts, opening of the ligand-gated ionotropic receptors on the postsynaptic cells, and generation of postsynaptic action potentials. It remains unknown how the central arc produces the derivative characteristics despite the synaptic delay. In electrical circuits, the derivative characteristics can be built from a delay element alone by introducing feedback [76]. A reciprocal neural connection is reported from the RVLM to the NTS [90]. If such a connection acts as a feedback path within the central arc, it could explain the generation of derivative characteristics.

Bionic baroreflex system

Once the dynamic transfer function of the total reflex arc, $H_T(f)$, is quantified, the arterial baroreflex function can be restored in cases of central baroreflex failure. In a study by Sato et al. [91], a bionic baroreflex system is proposed, in which a pressure sensor monitors AP and the bionic baroreflex center stimulates the efferent sympathetic nerve to mimic the normal baroreflex control of AP. First, the transfer function from celiac nerve stimulation to AP, $H_{\mathrm{stim}\rightarrow\mathrm{AP}}(f)$, was identified by a white noise analysis. Next, the transfer function of the bionic baroreflex center from pressure input to celiac nerve stimulation, $H_{\mathrm{bionic}}(f)$, was determined to fulfill the following equation:

$$H_{\mathrm{bionic}}(f)H_{\mathrm{stim}\rightarrow AP}(f) = H_{\mathrm{T}}(f) \tag{16}$$

This bionic baroreflex system is able to prevent orthostatic hypotension in a rat model of central baroreflex

failure [92]. Furthermore, Yanagiya et al. [93] showed that epidural spinal cord stimulation can be used as the efferent path of the bionic baroreflex system to control AP in anesthetized cats.

Hosokawa et al. [74], on the other hand, estimated the transfer function from aortic depressor nerve stimulation to AP, and then developed a bionic baroreceptor (not baroreflex) system. The system assumes preserved functioning of the central and peripheral pathways of the arterial baroreflex system. Although the idea of enhancing carotid sinus baroreflex by electrical stimulation is not new and dates back to 1958 [94], the bionic baroreceptor system may provide a safer and more adaptive blood pressure-lowering therapy for patients with drug-resistant hypertension if used in combination with baroreflex activation therapy [74, 95].

A bionic baroreflex system aims to restore the normal function of the native arterial baroreflex system. However, considering the fact that the ultimate goal of the arterial baroreflex system is to stabilize AP, an artificial controller may be designed without knowing exactly the transfer function of the total reflex arc. As an example, Yamasaki et al. [96], using a classic controller with proportional and integral gain factors, demonstrated the successful application of epidural spinal cord stimulation to maintain AP against a model of sudden hypotension during knee surgery in humans. Gotoh et al. [83], using a proportional–integral–differential controller, also demonstrated the ability of RVLM stimulation to control AP in conscious rats.

Closed-loop identification of open-loop dynamic characteristics

Erroneous application of open-loop analysis

When SNA and AP are measured under baroreflex closed-loop conditions, an ordinary transfer function analysis in the frequency domain yields an erroneous estimation of the open-loop transfer function [97] as discussed below. First, let us think about open-loop analysis of the carotid sinus baroreflex. Under baroreflex open-loop conditions, SNA is expressed in the frequency domain as:

$$\mathrm{SNA}(f) = H_{\mathrm{N}}(f)\mathrm{CSP}(f) + N(f) \tag{17}$$

where SNA(f), CSP(f), and $N(f)$ represent the Fourier transforms of SNA, CSP, and unknown central noise component in SNA, respectively; and $H_{\mathrm{N}}(f)$ is the neural arc transfer function. Calculating cross spectra between the terms of Eq. 17 and *CSP*(f) and averaging them over multiple segments yields the following equation:

$$E[\mathrm{SNA}(f)\mathrm{CSP}^*(f)] = H_{\mathrm{N}}(f)E[\mathrm{CSP}(f)\mathrm{CSP}^*(f)] + E[N(f)\mathrm{CSP}^*(f)] \tag{18}$$

where CSP*(f) denotes a complex conjugate of CSP(f). Because the system is supposed to be time invariant within a time frame of the study, $H_{\mathrm{N}}(f)$ is outside the ensemble averaging operation, $E(\cdot)$. When CSP is perturbed according to a white noise signal, $E[N(f)\mathrm{CSP}^*(f)]$ asymptotically diminishes because the white noise is statistically independent of other noises. Therefore, $H_{\mathrm{N}}(f)$ can be estimated as:

$$H_{\mathrm{N}}(f) = \frac{E[\mathrm{SNA}(f)\mathrm{CSP}^*(f)]}{E[\mathrm{CSP}(f)\mathrm{CSP}^*(f)]} \tag{19}$$

which is an alternative expression of Eq. 7.

When the baroreceptor regions are not isolated from systemic circulation, SNA may be expressed in the frequency domain as:

$$\mathrm{SNA}(f) = H_{\mathrm{N}}(f)\mathrm{AP}(f) + N(f) \tag{20}$$

where AP(f) represents the Fourier transform of AP. Calculating cross spectra between the terms of Eq. 20 and AP(f) and averaging them over multiple segments results in:

$$E[\mathrm{SNA}(f)\mathrm{AP}^*(f)] = H_N(f)E[\mathrm{AP}(f)\mathrm{AP}^*(f)] + E[N(f)\mathrm{AP}^*(f)] \tag{21}$$

where AP*(f) denotes a complex conjugate of AP(f). While Eq. 21 is similar to Eq. 18, $N(f)$ and AP(f) do not become statistically independent even when AP is perturbed according to a white noise signal because the unknown central noise component of SNA affects AP through the peripheral arc. Hence, $E[N(f)\mathrm{AP}^*(f)]$ does not diminish, and $H_{\mathrm{N}}(f)$ needs to be estimated as:

$$H_{\mathrm{N}}(f) = \frac{E[\mathrm{SNA}(f)\mathrm{AP}^*(f)] - E[N(f)\mathrm{AP}^*(f)]}{E[\mathrm{AP}(f)\mathrm{AP}^*(f)]} \tag{22}$$

Ignoring the effect of $E[N(f)\mathrm{AP}^*(f)]$ and using Eq. 19 by simply replacing CSP with AP results in a biased estimation of the transfer function. Unfortunately, Eq. 22 itself cannot be used for analyzing actual data because $N(f)$ is unknown.

Mathematical opening of closed loop

When AP is perturbed by blood withdrawal and reinfusion according to a known white noise signal, it may be possible to estimate the neural arc transfer function by mathematically opening the baroreflex closed loop as follows [27]. Calculating cross spectra between the terms of Eq. 20 and the Fourier transform of the command signal, CMD(f), and averaging them over multiple segments yields the following equation:

$$E[\mathrm{SNA}(f)\mathrm{CMD}^*(f)] = H_\mathrm{N}(f)E[\mathrm{AP}(f)\mathrm{CMD}^*(f)] + E[N(f)\mathrm{CMD}^*(f)] \quad (23)$$

where CMD*(f) denotes a complex conjugate of CMD(f). Because the externally applied white noise command signal should be independent of the unknown central noise component of SNA, $E[N(f)\mathrm{CMD}^*(f)]$ asymptotically diminishes even under baroreflex closed-loop conditions. Hence, $H_\mathrm{N}(f)$ can be estimated from the following equation [98]:

$$H_\mathrm{N}(f) = \frac{E[\mathrm{SNA}(f)\mathrm{CMD}^*(f)]}{E[\mathrm{AP}(f)\mathrm{CMD}^*(f)]} \quad (24)$$

Once $H_\mathrm{N}(f)$ is estimated, the unknown central noise component of SNA can be estimated from Eq. 20. The central noise component of SNA is then used to estimate the transfer function of the peripheral arc [27]. A merit of the closed-loop identification is that possible surgical damage to baroreceptor regions can be avoided. However, the dynamic AP perturbation by blood withdrawal and reinfusion is not likely feasible in conscious animals.

Partial closed-loop identification

As an alternative to the dynamic AP perturbation described in the previous section, SNA can be perturbed dynamically via aortic depressor nerve stimulation, which may possibly enable closed-loop identification [99]. Unfortunately, this method does not completely solve the closed-loop identification problem. That is to say, when SNA is perturbed, the peripheral arc transfer function can be estimated using the stimulation command signal. However, the unknown noise component of AP uncoupled with SNA is not large enough to allow for the estimation of the neural arc transfer function, at least under anesthetized conditions. To estimate the neural arc transfer function, AP also needs to be perturbed by another method that includes intermittent rapid pacing of the heart. Intermittent rapid pacing, on the other hand, allows the estimation of the neural arc but not the peripheral arc transfer function, though it is similar to the blood withdrawal and reinfusion in the sense it perturbs AP. This is because the intermittent rapid pacing interferes with normal cardiac function and significantly distorts the peripheral arc transfer function [99].

Dynamic AP perturbation using intermittent balloon inflation and deflation at the thoracic aorta may allow estimation of the neural arc transfer function from the AP input to SNA with reasonable accuracy [87, 100, 101]. This may also be because the intermittent balloon inflation and deflation significantly distort the peripheral arc transfer function and effectively sever the linear coupling between the unknown central noise component of SNA and AP. Nevertheless, using Eq. 24 might be a theoretically solid estimate of the neural arc transfer function under baroreflex closed-loop conditions.

Common limitations for closed-loop identification

There are several limitations common to all closed-loop identification methods and partial closed-loop identification. First, the arterial baroreflex function can be estimated only around the baseline operating-point AP under given conditions. Hence the nonlinear characteristics of the arterial baroreflex such as threshold and saturation phenomena are difficult to identify unless a very large perturbation is imposed. Second, the amplitude of AP perturbation cannot be controlled exactly under baroreflex closed-loop conditions. These two limitations may cause error when comparing the arterial baroreflex function among different conditions because the dynamic characteristics of the arterial baroreflex can change depending on the mean and amplitude of the input perturbation [77, 102]. It is difficult, without baroreceptor isolation, to impose a white noise signal with specific distribution properties such as Gaussian white noise, which limits the ability to estimate higher-order nonlinear dynamics of the system [4].

Integration with static characteristics

Cascade models

For convenience reasons, the dynamic characteristics of the arterial baroreflex system are described separately from the static characteristics in this article. However, the dynamic characteristics may need to be combined with the static characteristics to describe the overall baroreflex function. For both the neural and peripheral arcs, the simplest structure is a cascade connection of the static and dynamic characteristics. With respect to the peripheral arc, because the static characteristics are nearly linear, a static–dynamic cascade model and a dynamic–static cascade model are functionally indistinguishable. On the other hand, because the static characteristics of the neural arc are sigmoidal nonlinear in nature, a static–dynamic cascade model and a dynamic–static cascade model yield different dynamic transfer functions when activated with a binary white noise input. Based on experimental results, the dynamic–static cascade model has been previously suggested to be a better first approximation of the neural arc [77].

While the dynamic–static cascade model explains the operating point-dependence of the neural arc transfer function [102], this does not mean that the actual neural arc is so simple. In the dynamic–static cascade model, the range of SNA is exactly the same as that of the static characteristics determined from the steady-state SNA response. However, an abrupt reduction of CSP from 180

to 60 mmHg sometimes evokes a transient SNA elevation that exceeds the maximum value of the steady-state SNA response [31]. A staircase-wise increase of CSP from 80 to 100 mmHg or from 100 to 120 mmHg can transiently reduce SNA below the minimum value of the steady-state SNA response [67]. To describe these transient SNA responses, additional dynamic characteristics are required after the dynamic–static cascade model.

Parallel models

While the models of neural and peripheral arcs need to be described as a cascade connection, parallel connections of subsystems may also be considered to describe the overall function of the arterial baroreflex system. For instance, a model by Ursino et al. [103] divides the overall baroreflex function into parallel blocks representing the baroreflex effects on systemic peripheral resistance, heart period, and volume shift to the systemic circulation. A model by Sakamoto et al. [23] uses parallel blocks representing the transfer functions from CSP to left ventricular end-systolic elastance, CSP to HR, CSP to systemic peripheral resistance, and CSP to stressed blood volume, followed by blocks of the cardiac output curve and venous return surface to determine AP [104]. While the model by Sakamoto does not separate the neural and peripheral arc components or include the nonlinearity of the neural arc, it demonstrates a predominance of vascular properties, not ventricular properties, in baroreflex-mediated sympathetic AP regulation.

Volterra series

As an aside from the above-mentioned approaches, it may also be possible to describe the overall system characteristics without assuming any particular structure by using a Volterra series. For a finite memory causal system, the Volterra series is given as follows [105]:

$$\begin{aligned} y(t) = h_0 &+ \int_0^M h_1(\tau)x(t-\tau)\mathrm{d}\tau \\ &+ \int_0^M \int_0^M h_2(\tau_1,\tau_2)x(t-\tau_1)x(t-\tau_2)\mathrm{d}\tau_1\mathrm{d}\tau_2 \\ &+ \int_0^M \int_0^M \int_0^M h_3(\tau_1,\tau_2,\tau_3)x(t-\tau_1)x(t-\tau_2) \\ &\times x(t-\tau_3)\mathrm{d}\tau_1\mathrm{d}\tau_2\mathrm{d}\tau_3 + \cdots + \varepsilon(t) \end{aligned} \tag{25}$$

where $x(t)$ and $y(t)$ are the input and output of the system, respectively; $\varepsilon(t)$ represents the error of description. The equation is a generalization of Eq. 9, including the mean output value, h_0, the first-order kernel or impulse response, $h_1(\tau)$, the second-order kernel, $h_2(\tau_1, \tau_2)$, the third-order kernel, $h_3(\tau_1, \tau_2, \tau_3)$, and so on. M is the length of the system memory, which can be different for each kernel. The error magnitude $|\varepsilon(t)|$ can be made arbitrarily small by increasing the order of kernels. The Gaussian white noise input is efficient for estimating such higher-order nonlinearities of the system [4]. However, because the number of parameters exponentially increases with an increase in the order of kernels whereas the experimental data length is relatively short, nonlinear analysis is usually limited up to the second-order nonlinearity [106]. Given the presence of threshold and saturation nonlinearities, a nonlinear analysis beyond the second-order nonlinearity may be required to fully describe the arterial baroreflex function.

Effects of various interventions on open-loop baroreflex characteristics

Exogenous interventions

Angiotensin II

Angiotensin II is a powerful vasoconstrictor peptide and is thought to affect the baroreflex peripheral arc. Angiotensin II can also affect sympathetic AP regulation by centrally increasing sympathetic outflow, stimulating sympathetic ganglia and the adrenal medulla, and facilitating neurotransmission at the sympathetic nerve endings [107]. Figure 4 illustrates the baroreflex equilibrium diagram before and during intravenous administration of angiotensin II (10 μg kg^{-1} h^{-1}) in anesthetized rats [31]. As expected, angiotensin II causes an upward shift of the peripheral arc toward higher AP. The closed-loop operating point moves from point 'a' to point 'b' because angiotensin II also yields a rightward shift of the neural arc toward higher SNA. If the changes in the operating point alone were observed under baroreflex closed conditions, then angiotensin II would increase AP without a suppression of SNA, which might lead to an interpretation that angiotensin II impairs the neural arc function. In reality, changes in CSP from 60 to 180 mmHg can significantly reduce SNA under background infusion of angiotensin II, indicating that the neural arc function is maintained in terms of its responsiveness to input pressure change. It appears that angiotensin II increases the baroreflex-independent tonic component of SNA.

The dynamic transfer functions of the neural and peripheral arcs are not significantly affected by a pressor dose of intravenous angiotensin II (6 μg kg^{-1} h^{-1}) in anesthetized rabbits [108]. The insignificant effect of angiotensin II on the neural arc transfer function may be

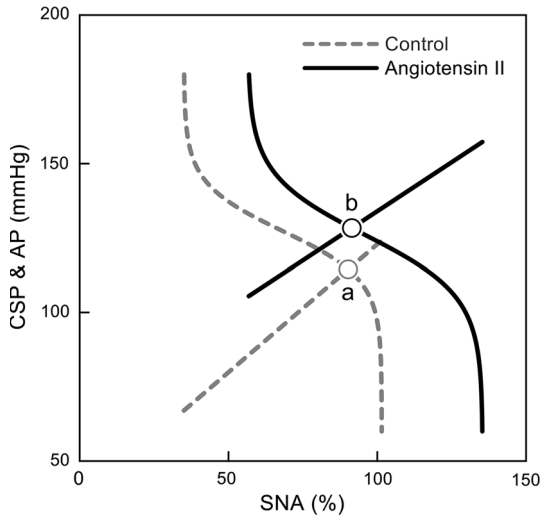

Fig. 4 Baroreflex equilibrium diagram obtained under control conditions (*gray broken line* and *curve*) and during intravenous administration of angiotensin II (*black solid line* and *curve*). *CSP* carotid sinus pressure, *AP* arterial pressure, *SNA* sympathetic nerve activity. Angiotensin II moves the operating point from point 'a' to point 'b'. If we observe the change in the operating point alone under baroreflex closed-loop conditions, angiotensin II increases AP but does not reduce SNA, which would lead to an interpretation that angiotensin II blunts the arterial baroreflex function. However, the baroreflex equilibrium diagram indicates that the neural arc resets to higher SNA without losing the ability to respond to changes in CSP (modified from Fig. 4 in Ref. 31 with permission)

consistent with previous findings that the derivative characteristics of the neural arc are preserved in disease models of chronic heart failure [67, 101] and hypertension [100, 109] where an increased level of central angiotensin II is considered to be a mechanism of excess sympathoexcitation [110–112].

Angiotensin II stimulates the production of superoxide and interacts with nitric oxide in the central nervous system [113]. Miyano et al. [114] examined the effects of inhibiting nitric oxide production on the dynamic characteristics of the carotid sinus baroreflex. Inhibition of nitric oxide production by an intravenous administration of N^G-monomethyl-L-arginine (L-NMMA) minimally affects the neural arc transfer function, suggesting that nitric oxide is mainly involved in tonic rather than dynamic regulation of SNA. The administration of L-NMMA does not affect the peripheral arc transfer function, indicating that basal nitric oxide release plays a minimal role in the dynamic sympathetic regulation of AP [115].

Head-up tilt

During a head-up tilt, blood pools in the lower extremities, which is considered to have effects similar to blood loss on the circulatory regulation. In a study by Kamiya et al. [116] using anesthetized rabbits, the head-up tilt causes a downward shift of the peripheral arc toward lower AP, which is consistent with the effect of blood loss. At the same time, the head-up tilt induces a rightward shift of the neural arc toward higher SNA, which keeps the operating-point AP relatively unchanged during the head-up tilt. While central command may increase SNA during spontaneous locomotion [117], it may not explain the resetting of the neural arc observed under anesthetic conditions.

Similar to the changes observed in the static characteristics, the dynamic gain of the peripheral arc transfer function is decreased, whereas the dynamic gain of the neural arc transfer function is increased during the head-up tilt [118]. Consequently, the dynamic gain of the total reflex arc transfer function is relatively unaffected by orthostatic stress. A simulation of the closed-loop AP response indicates that the resetting of the neural arc has a critical role in activating SNA and preventing hypotension during orthostatic stress not only in the static but also in the dynamic response.

Head-up tilt and vestibular lesion

While the resetting of the neural arc toward higher SNA contributes to the maintenance of AP during a head-up tilt, the mechanisms for resetting remain to be fully elucidated. One possible mechanism is input from the vestibular system. Abe et al. [119] examined the effects of sinoaortic baroreceptor denervation, vestibular lesion, or both, on AP during voluntary postural changes in conscious rats. Both the arterial baroreflex and vestibular systems contribute to the maintenance of AP during the voluntary rear-up.

Abe et al. [119] also examined the effects of vestibular lesion on the baroreflex equilibrium diagram in anesthetized rats. In agreement with the study in anesthetized rabbits [116], the head-up tilt caused a downward shift of the peripheral arc and a rightward shift of the neural arc in sham-operated rats. In contrast, resetting of the neural arc toward higher SNA was abolished in rats with vestibular lesion, and the operating-point AP was significantly decreased during the head-up tilt. These results suggest that the input from the vestibular system is an important source for resetting of the neural arc during orthostatic stress. The findings agree with a human study where activation of the otolith organs by a head-down rotation increases muscle SNA [120]. One caveat for the involvement of the vestibular reflex in providing a tolerance against the gravitational stress is that the vestibular reflex does not directly monitor AP and may evoke significant sympathoexcitation if the arterial baroreflex is disabled [121].

Passive muscle stretch

Mechanoreflex and metaboreflex from exercising muscles are thought to modify the arterial baroreflex function during exercise. Yamamoto et al. [64] examined the effects of passive muscle stretch on the baroreflex equilibrium diagram in anesthetized rabbits. A passive muscle stretch applied at the hind limb caused a rightward shift of the neural arc toward higher SNA without affecting the peripheral arc. Resetting of the neural arc induced by the muscle mechanoreflex might compensate for AP falls resulting from vasodilation in exercising muscles. Although the contribution of the mechanoreflex to the maintenance of AP during standing remains to be examined, afferent signals from the acting muscles could be another source for resetting of the neural arc toward higher SNA during orthostatic stress.

Muscle mechanoreflex induced by passive muscle stretch increases the dynamic gain of the neural arc transfer function but does not significantly affect the peripheral arc transfer function [76]. A simulation of the closed-loop AP response indicates that the muscle mechanoreflex may accelerate the AP regulation by increasing the dynamic gain of the total reflex arc.

Pharmacological afferent vagal nerve stimulation

Intravenous administration of veratrum alkaloids evokes cardioresipratory inhibitory responses known as the Bezold–Jarisch reflex. Serotonin 5-HT_3 receptors on the vagal sensory fibers may be involved in the Bezold–Jarisch reflex induced by intravenous phenylbiguanide [122]. Kashihara et al. [123] examined the effect of intravenous phenylbiguanide on the baroreflex equilibrium diagram in anesthetized rabbits with intact vagal nerves. The Bezold–Jarisch reflex caused a leftward shift of the neural arc toward lower SNA and decreased the slope of the peripheral arc. Consequently, the Bezold–Jarisch reflex decreased the operating-point SNA and AP. The suppression of SNA might not have been mediated by the direct central effect of phenylbiguanide because vagotomy abolished the shift in SNA. Afferent vagal nerve stimulation by phenylbiguanide may accompany efferent vagal nerve activation as evidenced by an increase in myocardial interstitial acetylcholine concentration in anesthetized cats [124]. Therefore, the observed changes in the baroreflex equilibrium diagram during the intravenous phenylbiguanide administration may be a combined result from activation of both the afferent and efferent pathways of the vagal nerves.

The Bezold–Jarisch reflex induced by intravenous phenylbiguanide decreases the dynamic gain of the neural arc transfer function but does not significantly affect the peripheral arc transfer function [125]. Excess activation of the Bezold–Jarisch reflex during acute myocardial ischemia may compromise the maintenance of AP, not only by sympathetic suppression but also by the impairment of the dynamic gain of the arterial baroreflex.

Electrical afferent vagal nerve stimulation

Saku et al. [37] examined the effects of electrical stimulation of the afferent pathway of the cut right vagal nerve on the baroreflex equilibrium diagram in anesthetized rats. Possible confounding reflex effects, such as those from low-pressure baroreflexes, were avoided because this experiment was performed following vagotomy. On the other hand, the effects may not be specific for cardiovascular regulation because electrical stimulation may activate all the fibers in the vagal nerve such as those directed to gastrointestinal organs. While the vagal nerve was stimulated at the neck region, it might have been a better protocol to stimulate the intrathoracic portion of the vagal nerve [126] to avoid contamination from possible aortic depressor nerve stimulation. While these limitations should be kept in mind, the study by Saku et al. [37] indicates that the electrical afferent vagal nerve stimulation causes a leftward shift of the neural arc toward lower SNA without significantly affecting the peripheral arc. As a result, afferent vagal nerve stimulation decreases the operating-point SNA and AP. This finding is qualitatively compatible with a study using a reversible carotid isolation procedure in conscious dogs [33] where vagotomy caused an upward shift in the CSP–AP relationship.

Electrical efferent vagal nerve stimulation

Electrical vagal nerve stimulation [127] or application of acetylcholine [128] inhibits noradrenaline release from the isolated perfused rabbit heart in response to electrical postganglionic sympathetic nerve stimulation. Interactions are known to exist between the sympathetic and vagal systems in regulating HR [50, 129]. However, whether efferent vagal nerve stimulation significantly modified the baroreflex-mediated sympathetic AP regulation remained unknown. To investigate this question, the effects of electrical stimulation of the efferent pathway of the cut right vagal nerve on the baroreflex equilibrium diagram were examined in anesthetized rats [38]. Efferent vagal nerve stimulation (20 Hz, 1–4 V, 2-ms pulse width) reduced HR by 58 beats/min (13 % of a baseline HR) and decreased the intercept of the peripheral arc by 5.8 mmHg and the operating-point AP by 2.8 mmHg. In contrast, the parameters of the neural arc and the total reflex arc were not changed significantly, suggesting a limited effect of the moderate vagal nerve stimulation to modify the baroreflex-mediated sympathetic AP regulation.

Several explanations can be put forward to explain the limited effect of the moderate vagal nerve stimulation to reduce AP. First, there is little efferent vagal innervation on the systemic resistance vessels, though blood flow within specific organs can be modulated by vagal nerve stimulation [130]. Second, although slowing HR by efferent vagal nerve stimulation should reduce cardiac output if stroke volume is unchanged, the reduction of HR may be partly counterbalanced by an increase in stroke volume. Third, the negative inotropic effect of vagal nerve stimulation on the left ventricle is not so strong because it is induced only indirectly by a slowing of HR [131] and by an antagonism to sympathetic regulation [132].

Although the results of the above study indicate that moderate vagal nerve stimulation has limited ability to reduce AP, the effects of the efferent vagal nerve stimulation on mean AP depends on the intensity of stimulation. When HR is reduced by approximately 80 beats/min by bilateral vagal nerve stimulation in anesthetized cats (a reduction of approximately 40 % of a baseline HR), mean AP is significantly decreased [133]. When the atrial rate is reduced by approximately 180 beats/min by right vagal nerve stimulation in anesthetized rabbits (a reduction of approximately 60 % of a baseline HR), mean AP is significantly decreased even when the ventricular rate is maintained [134]. In addition, the effects of efferent vagal nerve stimulation on AP may depend on the level of background SNA. As an example, a fixed intensity of bilateral vagal nerve stimulation (20 Hz, 5 V, 2-ms pulse width) reduces mean AP in spontaneously hypertensive rats but not in normotensive Wistar-Kyoto rats [135].

Electroacupuncture

Acupuncture has been shown to modulate autonomic nervous activity via somatic afferent stimulation [136, 137]. Acupuncture is an attractive treatment for autonomic imbalance in humans because it does not require surgery (i.e., an electrode implantation to interface with the autonomic nervous system). On the other hand, quantitative analysis is still lacking about the effects of acupuncture on circulatory regulation. Michikami et al. [66] examined the effects of electroacupuncture on the baroreflex equilibrium diagram in anesthetized rabbits. Electroacupuncture at the Zusanli acupuncture point of the hind limb caused a leftward shift of the neural arc toward lower SNA without a significant effect on the peripheral arc, resulting in the reductions of operating-point SNA and AP. Electroacupuncture is being explored as a complementary therapy for cardiovascular diseases because autonomic imbalance characterized by sympathoexcitation and vagal withdrawal is considered to be an aggravating factor in cardiovascular diseases such as heart failure, [138, 139].

A possible application of electroacupuncture for short-term AP control has been examined in anesthetized cats [140]. The transfer function from hind limb electroacupuncture to AP approximated a second-order low-pass filter with pure delay. By using the estimated model transfer function, a proportional–integral controller was designed so that the stimulation current and frequency of electroacupuncture were automatically determined to decrease AP to a predefined target level.

Calcium channel blockers

The baroreflex equilibrium diagram is useful to understand the effects of pharmacological agents on sympathetic AP regulation, because it enables separate estimation of the central and peripheral effects of a given drug. Nifedipine, a first generation dihydropyridine (DHP) L-type calcium channel blocker, decreases AP via vasodilation. The decrease in AP activates SNA through the arterial baroreflex and increases HR, which is known as reflex tachycardia. The second and third generations of DHP calcium channel blockers have been developed to avoid the reflex tachycardia. Although the slow onset of the drug effect contributes to the absence of reflex tachycardia in the second and third generations of DHP calcium channel blockers [141], the direct inhibition of SNA can be an auxiliary mechanism. To assess the direct drug effect on SNA independently of the baroreflex-mediated effect on SNA, Yamamoto et al. [142, 143] examined the effects of DHP calcium channel blockers on the baroreflex equilibrium diagram. The acute effect of DHP calcium channel blockers on the neural arc is minimal, and the hypotensive effect can primarily be attributable to a reduction in the slope of the peripheral arc. While SNA at a given CSP does not change significantly, the CSP–HR relationship shows a downward shift, suggesting a direct negative chronotropic effect of DHP L-type calcium channel blockers. Although the HR response is sometimes used as an index for the autonomic tone from the central nervous system, the HR data needs to be carefully interpreted when a given drug has a direct influence on the activity of the sinoatrial node.

Intravenous administration of an N-type calcium channel blocker ω-conotoxin GVIA nearly abolishes the AP response to SNA without a significant effect on the maximum SNA [142], which reflects the importance of N-type calcium channels in the noradrenaline release from the sympathetic nerve terminals [144]. Whereas the L-type calcium channel blockade spares the HR response to changes in CSP, the N-type calcium channel blockade nearly abolishes the HR response to changes in CSP.

Although the intravenous administration of nifedipine does not significantly affect the neural arc transfer function, it significantly reduces the dynamic gain of the peripheral

arc transfer function [145]. A simulation on the closed-loop AP response indicates that the nifedipine-induced reduction of dynamic gain nearly doubles the 80 % recovery time of the AP response to an exogenous step disturbance. It is possible that an overdose of L-type calcium channel blockers may compromise the rapid AP control by the arterial baroreflex system and prolong hypotensive events.

Disease models

Chronic heart failure

Arterial baroreflex function has been shown to be depressed in chronic heart failure (CHF). Under baroreflex closed-loop conditions, a decrease in AP due to decreased cardiac output in CHF can increase sympathetic outflow as a consequence of normal baroreflex operation. To determine whether the baroreflex function is truly impaired in CHF, baroreflex responses need to be examined using an identical pressure input under baroreflex open-loop conditions. In a study by White [20] using a canine model of low-output right heart failure, the baroreflex response range of AP is smaller in the CHF group than in the sham-operated control group before vagotomy. The difference in the AP response range becomes insignificant after vagotomy. In a study by Wang et al. [21] using a canine model of rapid pacing-induced heart failure, renal SNA and AP responses to CSP are attenuated in the CHF group. In contrast, the renal SNA response to electrical stimulation of the carotid sinus nerve is not different between the normal and CHF groups. In another study by Wang et al. [57], vagotomy does not significantly change the baroreflex responses to CSP or electrical stimulation of the carotid sinus nerve in either the sham-operated or CHF group under anesthetic conditions. Olivier and Stephenson [35] have demonstrated time-dependent depressions of the carotid sinus baroreflex after the initiation of rapid pacing (days 3 through 21) in conscious dogs. Attenuation of the response range and static gain of the total reflex arc are evident from day 3.

While the above-mentioned studies demonstrated impairment of arterial baroreflex function in CHF, they did not deal with how the operating point was changed in CHF. To address this issue, the baroreflex equilibrium diagram was compared between normal rats and rats with CHF after myocardial infarction in our laboratory [67]. With respect to the neural arc, the magnitude of maximum sympathetic suppression is impaired in the CHF group. Possible mechanisms for the sympathoexcitation include afferent signals from the failing heart [111], an effect of central angiotensin II [110], and a reduced reflex from cardiopulmonary region [146]. The maximum gain of the neural arc, however, is not significantly reduced in CHF compared with the normal group. With respect to the peripheral arc, the slope is smaller in CHF than in the normal group, indicating an impaired AP response to percent change in SNA. Despite the significant changes in the neural and peripheral arcs, the operating-point AP is only slightly decreased in the CHF compared with the normal group (116 ± 3 vs. 106 ± 3 mmHg, $p < 0.05$) without a significant difference in the total reflex gain at the operating point (1.23 ± 0.28 vs. 0.96 ± 0.39 mmHg/mmHg) [67].

Although the AP response to percent changes in SNA is impaired in CHF, normalization of SNA might have affected the assessment of the slope of the peripheral arc. If the sympathetic outflow is increased in CHF, the same percent of SNA may indicate larger absolute SNA. Hence, the slope of the peripheral arc in CHF could be much smaller if SNA is expressed in absolute units. Regarding this point, the slope of the AP response to exogenous phenylephrine or noradrenaline is reduced in rats with CHF compared with normal rats, such that the slope ratio is between 0.6 and 0.7 [68]. The slope of the AP response to preganglionic sympathetic nerve stimulation is also reduced to approximately 0.5-fold in rats with CHF compared with sham-operated rats [147]. These data can be used to recalibrate the abscissa of the baroreflex equilibrium diagram between the normal and CHF groups [68].

Although the derivative characteristics of the neural arc are preserved in rats with CHF after myocardial infarction, the dynamic gain of the peripheral arc transfer function is significantly decreased in the lower frequency range [67]. As a result, the dynamic transfer function of the total reflex arc is significantly depressed in CHF than in the normal group. Although the total reflex gain at the operating point is not significantly different between the two groups, a numerical simulation indicates that the reserve for AP buffering is lost in the CHF group. This may be the reason why patients with stable CHF are easily decompensated by perturbations such as a lack of adherence to fluid restrictions.

Li et al. demonstrated that chronic intermittent electrical vagal nerve stimulation improves the survival of rats with CHF after myocardial infarction [148]. When the effects on the static characteristics of the carotid sinus baroreflex are examined in rats with CHF, the chronic vagal nerve stimulation increases the response range of percent SNA, suggesting improved neural arc function [149]. However, the effect of the chronic vagal nerve stimulation on the total reflex arc is limited due to the lack of significant improvement of the AP response to percent SNA.

Hypertension

The arterial baroreflex control of AP resets to a higher pressure range in hypertension [150]. As an example,

Nosaka and Wang [28] examined the open-loop static characteristics of the carotid sinus baroreflex in spontaneously hypertensive rats (SHR). The CSP–AP relationship resets to a higher CSP range and also to a higher AP range. Although the threshold pressure of baroreceptor firing is increased in untreated SHR, antihypertensive treatment prevents baroreceptor resetting [151], suggesting that the resetting is secondary to the development of hypertension. A different study indicates, however, that baroreceptor resetting occurs without any reduction in aortic wall distensibility at 10 weeks of age when SHR has significantly elevated AP [152], indicating early hypertensive baroreceptor resetting is primarily due to a change in receptor properties. Thereafter, the aorta of SHR lacked the normal increase in distensibility from 10 to 20 weeks of age, resulting in the reduced distensibility compared with normotensive rats.

Sympathetic outflow from the central nervous system is considered to be increased in SHR. However, whether an increased sympathetic outflow or an increased vascular responsiveness contributes more significantly to the AP elevation in SHR remains controversial, partly due to the lack of a proper methodology to quantify the absolute level of SNA [153]. To investigate the above problem, Sata et al. [69] examined the baroreflex equilibrium diagrams of SHR and normotensive Wistar-Kyoto rats (WKY). To compare SNA between the different groups, the abscissa of the baroreflex equilibrium diagram was rescaled based on the pressor response to graded doses of intravenous administration of phenylephrine. The relationship of steady-state AP response versus the logarithmic dose of phenylephrine did not differ significantly between WKY and SHR, which is in agreement with no significant difference in the cumulative concentration–response curve of phenylephrine in an in vitro ring preparation of the aorta isolated from WKY and SHR [154]. The results also agree with a previous report using pithed preparation where WKY and SHR had an equal sensitivity of the vasoconstrictor response to endogenous noradrenaline during thoracolumbar sympathetic stimulation up to submaximal frequencies [155]. After the rescaling of the abscissa, the baroreflex equilibrium diagram indicates that the AP elevation in SHR is predominantly mediated by the neural arc [69]. While the pathogenesis of hypertension is diverse and SHR does not represent all types of hypertension, the baroreflex equilibrium diagram in SHR reinforces the importance of the central nervous system as a treatment target for hypertension [156].

Unbalance between the formation and disposition of reactive oxygen species causes oxidative stress, which is one of the mechanisms of the increased sympathetic outflow in SHR. When an inorganic free radical scavenger tempol is microinjected into the RVLM, stroke-prone SHR shows a dose-dependent reduction in AP, suggesting the importance of oxidative stress in determining the sympathetic outflow [157]. This does not mean, however, that the oxidative redox signaling is unimportant in the normal AP regulation. When the effects of an intravenous tempol on the baroreflex equilibrium diagram were examined in our laboratory, the neural arc showed a leftward shift toward lower SNA in both WKY and SHR [158]. Therefore, oxidative redox signaling may be an intrinsic mechanism in the signal transduction of the arterial baroreflex system, and in SHR the signaling is enhanced, which induces pathological sympathoexcitation. Intravenous tempol slightly decreases the peripheral arc toward lower AP in SHR but not in WKY, suggesting that oxidative stress in the vasculature partly contributes to the elevation of AP in SHR.

The derivative characteristics of the neural arc transfer function are preserved in SHR [100, 109], indicating that the dynamic AP control against acute pressure disturbance is relatively preserved around the operating-point AP despite the elevation. While angiotensin II is one of the possible mechanisms for the sympathoexcitation in SHR [112], it does not significantly affect dynamic characteristics of the carotid sinus baroreflex [108]. Another possible explanation for the preserved derivative characteristics of the neural arc is that the sustained SNA response is mainly mediated by unmyelinated C-fiber baroreceptors whereas the transient response is mediated by myelinated A-fiber baroreceptors [42, 88, 89]. A recent study from our laboratory has indicated that the difference in the dynamic characteristics between A- and C-fiber central pathways is less evident in SHR compared with WKY [159]. In diseased conditions such as SHR, C-fibers may be more easily damaged by oxidative stress compared with A-fibers, resulting in the preserved transient response of SNA. Further studies are required to confirm this speculation.

Metabolic syndrome

Metabolic syndrome is a major public health problem. A decrease in arterial compliance is observed in obese subjects and animals, which could lead to the impairment of arterial baroreflex function due to the reduced distensibility of the arterial wall around baroreceptors. The impaired baroreflex function may cause impaired sodium excretion via an insufficient inhibition of renal SNA, which would eventually lead to volume expansion and hypertension. Abe et al. [160] tested this hypothesis by loading hyperosmotic NaCl solution in rats fed a high-fat diet and a normal diet. The rats fed a high-fat diet were divided into higher (Fat) and lower (Lean) body weight groups. The increase in AP, water balance, and sodium balance during 9 % NaCl loading were significantly larger in the Fat group

compared with the Lean and normal groups. The baroreflex equilibrium diagram shows a shift of the neural arc toward higher CSP in the Fat group. The peripheral arc shows a slight upward shift in the Fat and Lean groups compared with the normal group, suggesting that the AP intercept is increased by volume expansion. These changes result in a significantly higher operating-point AP in the Fat group than the other two groups. Although the comparison of absolute SNA among different groups is difficult due to the normalization of SNA, a higher noradrenaline excretion in urine is suggestive of higher absolute SNA in the Fat group. In the same study, the distensibility of the common carotid artery is shown to be reduced in the Fat group, suggesting that the shift of the neural arc induced by the reduced distensibility of the arterial wall around baroreceptors might contribute to the impairment of the sodium regulation in the Fat group.

Although causality of baroreceptor resetting in the genesis of hypertension cannot be definitively determined, the presence of decreased distensibility of the arterial wall in a model of metabolic syndrome may provide a rationale for the use of electrical activation of the baroreflex, which bypasses the mechano–neural transduction at the arterial baroreceptors, for the treatment of drug-resistant hypertension discussed in the following section [95].

Recent topics in relation to chronic arterial pressure regulation

In a classical view, the arterial baroreflex system is categorized as an acute AP regulating system that starts to operate in a few seconds and develops its maximum effect within a few minutes after a disturbance. This is partly because a study by Cowley et al. [161] demonstrated that the AP elevation following the sinoaortic baroreceptor denervation became insignificant within a few days in dogs. The variability of AP, on the other hand, remained increased after the sinoaortic baroreceptor denervation. Therefore, the primary purpose of the arterial baroreflex system has been believed to be the stabilization of AP against acute pressure disturbance and not the sustained control of the mean level of AP. The inability of the arterial baroreflex in controlling long-term AP is also considered to be related to the fact that the arterial baroreflex resets to a new prevailing pressure. Both the baroreceptors themselves and the baroreflex central pathway are involved in the resetting of the arterial baroreflex [162].

It has been recently reported that exposing the baroreceptors to lower perfusion pressure and lower pulse pressure, i.e., baroreceptor unloading, can induce hypertension for a longer period than ever thought before [163]. In contrast to the sinoaortic baroreceptor denervation, which might cause atrophy of synaptic connections in the central nervous system because of disuse, baroreceptor unloading may maintain the integrity of the baroreflex central pathway. In addition, electrical stimulation of baroreceptor afferent fibers has been shown to reduce AP for more than a week in dogs [164]. Bypassing the mechano–neural transduction at the arterial baroreceptors may contribute to avoiding the resetting at the baroreceptor level. Based on these findings, electrical activation of the arterial baroreflex is explored as a new therapy against drug-resistant hypertension [95].

The idea of electrical stimulation of the arterial baroreflex dates back to the 1960s when the method was used for pain relief from angina pectoris [165]. Electrical stimulation of the carotid sinus nerves in man decreased mean arterial pressure, on average, by 23 % [166]. Baroreflex activation therapy (BAT), however, remained experimental because of the development of new, effective drugs for the treatment of cardiovascular diseases including angina pectoris and hypertension. Nevertheless, the above-mentioned findings regarding the possible long-term regulation of AP by the arterial baroreflex, coupled with advancements in device technology (e.g., miniaturization of electric circuits) has motivated investigators to re-explore the use of BAT for the treatment of drug-resistant hypertension [95]. While carotid body chemoreceptors exist nearby, carotid sinus BAT does not seem to elicit chemoreflexes [167]. Chronic baroreceptor activation is also reported to enhance the survival of dogs with rapid pacing-induced heart failure [168], and to improve left ventricular function and promote reversal of left ventricular remodeling in dogs with coronary microembolization-induced heart failure [169]. Clinical application of BAT for heart failure with reduced ejection fraction is also reported [170].

The reason why the electrical activation of the arterial baroreflex can be more effective than pharmacological sympathetic blockade remains to be clarified. Several potential mechanisms are as follows. First, compliance with medication is not needed for BAT once the device has been implanted. Second, not only sympathetic suppression but also vagal activation is expected by BAT. While the significance of vagal activation in the treatment of hypertension is unknown, vagal activation is beneficial for the treatment of chronic heart failure [148]. Third, neural regulation is much stronger than the pharmacological intervention. For instance, 2-Hz cardiac sympathetic nerve stimulation is comparable to increasing a plasma noradrenaline concentration to approximately tenfold in its effects on a myocardial interstitial noradrenaline concentration and ventricular contractility in anesthetized cats [171]. The sympathetic HR response is robustly observed even when plasma catecholamine levels are increased to

approximately tenfold by intravenous catecholamine infusion in anesthetized rabbits [172]. These results imply that the concentration of sympathetic blockers at the synaptic clefts may not be sufficiently increased to antagonize high levels of SNA in patients with drug-resistant hypertension. In contrast, BAT may be able to suppress SNA more effectively because of its direct upstream intervention in the neural pathway.

Conclusions

The arterial baroreflex system has been and will be an important target of studies regarding autonomic and circulatory physiology, pathology, pharmacology, and medical treatments. Whole body animal experiments are still required to understand the arterial baroreflex function as a key link between the autonomic nervous system and the cardiovascular system. There is still a lack of information regarding the effects of many important physiologically active substances and pharmacological agents on the baroreflex equilibrium diagram. Interactions of the arterial baroreflex system with other reflex systems such as the chemoreflex remain to be fully elucidated. There are many disease models in which the baroreflex equilibrium diagram needs to be estimated for a better understanding of the underlying pathology. Observational studies alone do not allow quantitative description of the neural and peripheral arc characteristics because of the closed-loop operation of the arterial baroreflex and the presence of other parallel feedback systems. Despite known limitations such as the need for anesthesia and vagotomy, open-loop systems analyses of the static and dynamic characteristics need to be performed to fully understand the AP regulation via the arterial baroreflex system.

Acknowledgments The authors thank Dr. Michael J. Turner for his assistance with a native English check.

References

1. Sagawa K (1983) Baroreflex control of systemic arterial pressure and vascular bed. In: Shepherd JT, Abboud FM, Geiger SR (eds) Handbook of physiology. The cardiovascular system: peripheral circulation and organ blood flow, section 2, vol III, chapter 14. American Physiological Society, Bethesda, pp 453–496
2. Mohrman DE, Heller LJ (2010) Cardiovascular physiology, 7th edn. McGraw-Hill, New York, pp 246–250
3. Sato T, Kawada T, Inagaki M, Shishido T, Takaki H, Sugimachi M, Sunagawa K (1999) New analytic framework for understanding sympathetic baroreflex control of arterial pressure. Am J Physiol 276:H2251–H2261
4. Marmarelis PZ, Marmarelis VZ (1978) The white noise method in system identification. In: Analysis of physiological systems. Plenum, New York, pp 131–180
5. Bendat JS, Piersol AG (2010) Random data: analysis and measurement procedures, 4th edn. Wiley, New Jersey
6. Kumada M, Terui N, Kuwaki T (1990) Arterial baroreceptor reflex: its central and peripheral neural mechanisms. Prog Neurobiol 35:331–361
7. Hébert MT, Marshall JM (1988) Direct observation of effects of baroreceptor stimulation on mesenteric circulation of the rat. J Physiol 400:29–44
8. Agarwal SK, Calaresu FR (1992) Electrical stimulation of nucleus tractus solitarius excites vagal preganglionic cardiomotor neurons of the nucleus ambiguus in rats. Brain Res 574:320–324
9. Jordan D (2005) Vagal control of the heart: central serotonergic (5-HT) mechanisms. Exp Physiol 90:175–181
10. Zhang X, Abdel-Rahman AA, Wooles WR (1989) Impairment of baroreceptor reflex control of heart rate but not sympathetic efferent discharge by central neuroadministration of ethanol. Hypertension 14:282–292
11. Persson PB (1991) History of arterial baroreceptor reflexes. In: Persson PB, Kirchheim HR (eds) Baroreceptor reflexes: integrative function and clinical aspects. Springer, Berlin, pp 1–8
12. Wright S (1932) A lecture on recent work on the afferent control of the circulation in health and disease. Br Med J 1:457–462
13. Neil E (1961) Carl Ludwig and his pupils. Circ Res 9:971–978
14. Kalia M, Welles RV (1980) Brain stem projections of the aortic nerve in the cat: a study using tetramethyl benzidine as the substrate for horseradish peroxidase. Brain Res 188:23–32
15. Zimmer HG (2004) Heinrich Ewald Hering and the carotid sinus reflex. Clin Cardiol 27:485–486
16. Berger AJ (1980) The distribution of the cat's carotid sinus nerve afferent and efferent cell bodies using the horseradish peroxidase technique. Brain Res 190:309–320
17. Ikeda Y, Kawada T, Sugimachi M, Kawaguchi O, Shishido T, Sato T, Miyano H, Matsuura W, Alexander J Jr, Sunagawa K (1996) Neural arc of baroreflex optimizes dynamic pressure regulation in achieving both stability and quickness. Am J Physiol 271:H882–H890
18. Moissejeff E (1926) Zur Kenntnis des Carotissinusreflexes. Z Ges Exp Med 53:696–704
19. Schmidt RM, Kumada M, Sagawa K (1971) Cardiac output and total peripheral resistance in carotid sinus reflex. Am J Physiol 221:480–487
20. White CW (1981) Abnormalities in baroreflex control of heart rate in canine heart failure. Am J Physiol 240:H793–H799
21. Wang W, Chen JS, Zucker IH (1991) Carotid sinus baroreceptor reflex in dogs with experimental heart failure. Circ Res 68:1294–1301
22. Kawada T, Fujiki N, Hosomi H (1992) Systems analysis of the carotid sinus baroreflex system using a sum-of-sinusoidal input. Jpn J Physiol 42:15–34
23. Sakamoto T, Kakino T, Sakamoto K, Tobushi T, Tanaka A, Saku K, Hosokawa K, Onitsuka K, Murayama Y, Tsutsumi T, Ide T, Sunagawa K (2015) Changes in vascular properties, not ventricular properties, predominantly contribute to baroreflex regulation of arterial pressure. Am J Physiol Heart Circ Physiol 308:H49–H58
24. Ishikawa N, Sagawa K (1983) Nonlinear summation of depressor effects of carotid sinus pressure changes and aortic nerve stimulation in the rabbit. Circ Res 52:401–410
25. Chen HI, Bishop VS (1983) Baroreflex open-loop gain and arterial pressure compensation in hemorrhagic hypotension. Am J Physiol 245:H54–H59

26. Yamazaki T, Sagawa K (1989) Summation of sinoaortic baroreflexes depends on size of input signals. Am J Physiol 257:H465–H472
27. Kawada T, Sugimachi M, Sato T, Miyano H, Shishido T, Miyashita H, Yoshimura R, Takaki H, Alexander J Jr, Sunagawa K (1997) Closed-loop identification of carotid sinus baroreflex open-loop transfer characteristics in rabbits. Am J Physiol 273:H1024–H1031
28. Nosaka S, Wang SC (1972) Carotid sinus baroreceptor functions in the spontaneously hypertensive rat. Am J Physiol 222:1079–1084
29. Shoukas AA, Callahan CA, Lash JM, Haase EB (1991) New technique to completely isolate carotid sinus baroreceptor regions in rats. Am J Physiol 260:H300–H303
30. Sato T, Kawada T, Miyano H, Shishido T, Inagaki M, Yoshimura R, Tatewaki T, Sugimachi M, Alexander J Jr, Sunagawa K (1999) New simple methods for isolating baroreceptor regions of carotid sinus and aortic depressor nerves in rats. Am J Physiol 276:H326–H332
31. Kawada T, Kamiya A, Li M, Shimizu S, Uemura K, Yamamoto H, Sugimachi M (2009) High levels of circulating angiotensin II shift the open-loop baroreflex control of splanchnic sympathetic nerve activity, heart rate and arterial pressure in anesthetized rats. J Physiol Sci 59:447–455
32. Stephenson RB, Donald DE (1980) Reversible vascular isolation of carotid sinuses in conscious dogs. Am J Physiol 238:H809–H814
33. Stephenson RB, Donald DE (1980) Reflex from isolated carotid sinuses of intact and vagotomized conscious dogs. Am J Physiol 238:H815–H822
34. Tan W, Panzenbeck MJ, Hajdu MA, Zucker IH (1989) A central mechanism of acute baroreflex resetting in the conscious dog. Circ Res 65:63–70
35. Olivier NB, Stephenson RB (1993) Characterization of baroreflex impairment in conscious dogs with pacing-induced heart failure. Am J Physiol 265:R1132–R1140
36. McKeown KP, Shoukas AA (1998) Chronic isolation of carotid sinus baroreceptor region in conscious normotensive and hypertensive rats. Am J Physiol 275:H322–H329
37. Saku K, Kishi T, Sakamoto K, Hosokawa K, Sakamoto T, Murayama Y, Kakino T, Ikeda M, Ide T, Sunagawa K (2014) Afferent vagal nerve stimulation resets baroreflex neural arc and inhibits sympathetic nerve activity. Physiol Rep 2:e12136
38. Kawada T, Shimizu S, Li M, Kamiya A, Uemura K, Sata Y, Yamamoto H, Sugimachi M (2011) Contrasting effects of moderate vagal stimulation on heart rate and carotid sinus baroreflex-mediated sympathetic arterial pressure regulation in rats. Life Sci 89:498–503
39. Allison JL, Sagawa K, Kumada M (1969) An open-loop analysis of the aortic arch barostatic reflex. Am J Physiol 217:1576–1584
40. Okada H (1964) Reflex responses to stimulation of baroreceptors in the right subclavian artery. Am J Physiol 206:918–922
41. Sato T, Kawada T, Shishido T, Miyano H, Inagaki M, Miyashita H, Sugimachi M, Knuepfer MM, Sunagawa K (1998) Dynamic transduction properties of in situ baroreceptors of rabbit aortic depressor nerve. Am J Physiol 274:H358–H365
42. Turner MJ, Kawada T, Shimizu S, Fukumitsu M, Sugimachi M (2015) Open-loop characteristics of the arterial baroreflex after blockade of unmyelinated baroreceptors with resiniferatoxin. Auton Neurosci (**in press**)
43. Kobayashi M, Cheng ZB, Tanaka K, Nosaka S (1999) Is the aortic depressor nerve involved in arterial chemoreflexes in rats? J Auton Nerv Syst 78:38–48
44. Hirooka Y, Imaizumi T, Sugimachi M, Takeshita A (1992) Mechanisms involved in aortic baroreceptor excitation during drug-induced aortic pressure elevation in intact rabbits. J Auton Nerv Syst 40:99–106
45. Sato T, Kawada T, Inagaki M, Shishido T, Sugimachi M, Sunagawa K (2003) Dynamics of sympathetic baroreflex control of arterial pressure in rats. Am J Physiol Regul Integr Comp Physiol 285:R262–R270
46. Mancia G, Ferrari A, Gregorini L, Valentini R, Ludbrook J, Zanchetti A (1977) Circulatory reflexes from carotid and extracarotid baroreceptor areas in man. Circ Res 41:309–315
47. Ludbrook J, Mancia G, Ferrari A, Zanchetti A (1977) The variable-pressure neck-chamber method for studying the carotid baroreflex in man. Clin Sci Mol Med 53:165–171
48. Kawada T, Inagaki M, Takaki H, Sato T, Shishido T, Tatewaki T, Yanagiya Y, Sugimachi M, Sunagawa K (2000) Counteraction of aortic baroreflex to carotid sinus baroreflex in a neck suction model. J Appl Physiol 89:1979–1984
49. Berger RD, Saul JP, Cohen RJ (1989) Transfer function analysis of autonomic regulation. I. Canine atrial rate response. Am J Physiol 256:H142–H152
50. Kawada T, Ikeda Y, Sugimachi M, Shishido T, Kawaguchi O, Yamazaki T, Alexander J Jr, Sunagawa K (1996) Bidirectional augmentation of heart rate regulation by autonomic nervous system in rabbits. Am J Physiol 271:H288–H295
51. Hosomi H (1978) Overall characteristics of arterial pressure control system studied by mild hemorrhage. Am J Physiol 234:R104–R109
52. Hosomi H, Katsuda S, Morita H, Nishida Y, Koyama S (1986) Interactions among reflex compensatory systems for posthemorrhage hypotension. Am J Physiol 250:H944–H953
53. Suga H, Oshima M (1971) Measurement of the transfer function of the carotid sinus pressure control system with its feedback loop physiologically closed. Med Biol Eng 9:147–150
54. Schmidt RM, Kumada M, Sagawa K (1972) Cardiovascular responses to various pulsatile pressures in the carotid sinus. Am J Physiol 223:1–7
55. Chapleau MW, Abboud FM (1987) Contrasting effects of static and pulsatile pressure on carotid baroreceptor activity in dogs. Circ Res 61:648–658
56. Kawada T, Uemura K, Kashihara K, Jin Y, Li M, Zheng C, Sugimachi M, Sunagawa K (2003) Uniformity in dynamic baroreflex regulation of left and right cardiac sympathetic nerve activities. Am J Physiol Regul Integr Comp Physiol 284:R1506–R1512
57. Wang W, Brändle M, Zucker IH (1993) Influence of vagotomy on the baroreflex sensitivity in anesthetized dogs with experimental heart failure. Am J Physiol 265:H1310–H1317
58. Kawada T, Shimizu S, Sata Y, Kamiya A, Sunagawa K, Sugimachi M (2011) Consideration on step duration to assess open-loop static characteristics of the carotid sinus baroreflex in rats. Conf Proc IEEE Eng Med Biol Soc 2011:689–692
59. Kent BB, Drane JW, Blumenstein B, Manning JW (1972) A mathematical model to assess changes in the baroreceptor reflex. Cardiology 57:295–310
60. McDowall LM, Dampney RA (2006) Calculation of threshold and saturation points of sigmoidal baroreflex function curves. Am J Physiol Heart Circ Physiol 291:H2003–H2007
61. Ishikawa N, Kallman CH, Sagawa K (1984) Rabbit carotid sinus reflex under pentobarbital, urethane, and chloralose anesthesia. Am J Physiol 246:H696–H701
62. Kumada M, Schramm LP, Altmansberger RA, Sagawa K (1975) Modulation of carotid sinus baroreceptor reflex by hypothalamic defense response. Am J Physiol 228:34–45
63. Burattini R, Socionovo G, Bellocchi F (1994) On the approximation of static open-loop characteristics of baroreceptor reflex. Am J Physiol 267:H267–H275

64. Yamamoto K, Kawada T, Kamiya A, Takaki H, Miyamoto T, Sugimachi M, Sunagawa K (2004) Muscle mechanoreflex induces the pressor response by resetting the arterial baroreflex neural arc. Am J Physiol Heart Circ Physiol 286:H1382–H1388
65. Yamamoto K, Kawada T, Kamiya A, Takaki H, Sugimachi M, Sunagawa K (2005) Static interaction between muscle mechanoreflex and arterial baroreflex in determining efferent sympathetic nerve activity. Am J Physiol Heart Circ Physiol 289:H1604–H1609
66. Michikami D, Kamiya A, Kawada T, Inagaki M, Shishido T, Yamamoto K, Ariumi H, Iwase S, Sugenoya J, Sunagawa K, Sugimachi M (2006) Short-term electroacupuncture at Zusanli resets the arterial baroreflex neural arc toward lower sympathetic nerve activity. Am J Physiol Heart Circ Physiol 291:H318–H326
67. Kawada T, Li M, Kamiya A, Shimizu S, Uemura K, Yamamoto H, Sugimachi M (2010) Open-loop dynamic and static characteristics of the carotid sinus baroreflex in rats with chronic heart failure after myocardial infarction. J Physiol Sci 60:283–298
68. Kawada T, Li M, Sata Y, Zheng C, Turner MJ, Shimizu S, Sugimachi M (2015) Calibration of baroreflex equilibrium diagram based on exogenous pressor agents in chronic heart failure rats. Clin Med Insights Cardiol 9(Suppl 1):1–9
69. Sata Y, Kawada T, Shimizu S, Kamiya A, Akiyama T, Sugimachi M (2015) Predominant role of neural arc in sympathetic baroreflex resetting of spontaneously hypertensive rats. Circ J 79:592–599
70. Kawada T, Shishido T, Inagaki M, Zheng C, Yanagiya Y, Uemura K, Sugimachi M, Sunagawa K (2002) Estimation of baroreflex gain using a baroreflex equilibrium diagram. Jpn J Physiol 52:21–29
71. Fujiki N, Kawada T, Uemura N, Nishida Y, Morita H, Hosomi H (1993) Sulfite suppresses transducer function of the carotid sinus baroreceptor. J Auton Nerv Syst 43:139–150
72. Kawada T, Yamamoto K, Kamiya A, Ariumi H, Michikami D, Shishido T, Sunagawa K, Sugimachi M (2005) Dynamic characteristics of carotid sinus pressure-nerve activity transduction in rabbits. Jpn J Physiol 55:157–163
73. Kawada T, Shishido T, Inagaki M, Tatewaki T, Zheng C, Yanagiya Y, Sugimachi M, Sunagawa K (2001) Differential dynamic baroreflex regulation of cardiac and renal sympathetic nerve activities. Am J Physiol Heart Circ Physiol 280:H1581–H1590
74. Hosokawa K, Ide T, Tobushi T, Sakamoto K, Onitsuka K, Sakamoto T, Fujino T, Saku K, Sunagawa K (2012) Bionic baroreceptor corrects postural hypotension in rats with impaired baroreceptor. Circulation 126:1278–1285
75. Kawada T, Sato T, Shishido T, Inagaki M, Tatewaki T, Yanagiya Y, Sugimachi M, Sunagawa K (1999) Summation of dynamic transfer characteristics of left and right carotid sinus baroreflexes in rabbits. Am J Physiol 277:H857–H865
76. Yamamoto K, Kawada T, Kamiya A, Takaki H, Shishido T, Sunagawa K, Sugimachi M (2008) Muscle mechanoreflex augments arterial baroreflex-mediated dynamic sympathetic response to carotid sinus pressure. Am J Physiol Heart Circ Physiol 295:H1081–H1089
77. Kawada T, Yanagiya Y, Uemura K, Miyamoto T, Zheng C, Li M, Sugimachi M, Sunagawa K (2003) Input-size dependence of the baroreflex neural arc transfer characteristics. Am J Physiol Heart Circ Physiol 284:H404–H415
78. Bendat JS (1990) Zero-memory nonlinear systems. Nonlinear system analysis and identification from random data. Wiley, New York, pp 15–73
79. Kawada T, Zheng C, Yanagiya Y, Uemura K, Miyamoto T, Inagaki M, Shishido T, Sugimachi M, Sunagawa K (2002) High-cut characteristics of the baroreflex neural arc preserve baroreflex gain against pulsatile pressure. Am J Physiol Heart Circ Physiol 282:H1149–H1156
80. Kawada T, Miyamoto T, Uemura K, Kashihara K, Kamiya A, Sugimachi M, Sunagawa K (2004) Effects of neuronal norepinephrine uptake blockade on baroreflex neural and peripheral arc transfer characteristics. Am J Physiol Regul Integr Comp Physiol 286:R1110–R1120
81. Nakahara T, Kawada T, Sugimachi M, Miyano T, Sato T, Shishido T, Yoshimura R, Miyashita H, Inagaki M, Alexander J Jr, Sunagawa K (1999) Neuronal uptake affects dynamic characteristics of heart rate response to sympathetic stimulation. Am J Physiol 277:R140–R146
82. Mizuno M, Kawada T, Kamiya A, Miyamoto T, Shimizu S, Shishido T, Smith SA, Sugimachi M (2010) Dynamic characteristics of heart rate control by the autonomic nervous system in rats. Exp Physiol 95:919–925
83. Gotoh TM, Tanaka K, Morita H (2005) Controlling arterial blood pressure using a computer–brain interface. NeuroReport 16:343–347
84. Nakahara T, Kawada T, Sugimachi M, Miyano H, Sato T, Shishido T, Yoshimura R, Miyashita H, Inagaki M, Alexander J Jr, Sunagawa K (1998) Accumulation of cAMP augments dynamic vagal control of heart rate. Am J Physiol 275:H562–H567
85. Levison WH, Barnett GO, Jackson WD (1966) Nonlinear analysis of the baroreceptor reflex system. Circ Res 18:673–682
86. Kubo T, Imaizumi T, Harasawa Y, Ando S, Tagawa T, Endo T, Shiramoto M, Takeshita A (1996) Transfer function analysis of central arc of aortic baroreceptor reflex in rabbits. Am J Physiol 270:H1054–H1062
87. Harada S, Ando S, Imaizumi T, Hirooka Y, Sunagawa K, Takeshita A (1991) Arterial baroreflex control of cardiac and renal sympathetic nerve activities is uniform in frequency domain. Am J Physiol 261:R296–R300
88. Douglas WW, Ritchie JM, Schaumann W (1956) Depressor reflexes from medullated and non-medullated fibres in the rabbit's aortic nerve. J Physiol 132:187–198
89. Turner MJ, Kawada T, Shimizu S, Sugimachi M (2014) Sustained reduction in blood pressure from electrical activation of the baroreflex is mediated via the central pathway of unmyelinated baroreceptors. Life Sci 106:40–49
90. Agarwal SK, Calaresu FR (1990) Reciprocal connections between nucleus tractus solitarii and rostral ventrolateral medulla. Brain Res 523:305–308
91. Sato T, Kawada T, Shishido T, Sugimachi M, Alexander J Jr, Sunagawa K (1999) Novel therapeutic strategy against central baroreflex failure. Circulation 100:299–304
92. Sato T, Kawada T, Sugimachi M, Sunagawa K (2002) Bionic technology revitalizes native baroreflex function in rats with baroreflex failure. Circulation 106:730–734
93. Yanagiya Y, Sato T, Kawada T, Inagaki M, Tatewaki T, Zheng C, Kamiya A, Takaki H, Sugimachi M, Sunagawa K (2004) Bionic epidural stimulation restores arterial pressure regulation during orthostasis. J Appl Physiol 97:984–990
94. Warner HR (1958) The frequency-dependent nature of blood pressure regulation by the carotid sinus studied with an electric analog. Circ Res 6:35–40
95. Bakris GL, Nadim MK, Haller H, Lovett EG, Schafer JE, Bisognano JD (2012) Baroreflex activation therapy provides durable benefit in patients with resistant hypertension: results of long-term follow-up in the Rheos Pivotal Trial. J Am Soc Hypertens 6:152–158
96. Yamasaki F, Ushida T, Yokoyama T, Ando M, Yamashita K, Sato T (2006) Artificial baroreflex: clinical application of a bionic baroreflex system. Circulation 113:634–639

97. Kamiya A, Kawada T, Shimizu S, Sugimachi M (2011) Closed-loop spontaneous baroreflex transfer function is inappropriate for system identification of neural arc but partly accurate for peripheral arc: predictability analysis. J Physiol 589:1769–1790
98. Söderström T, Stoica P (1989) Identification of systems operating in closed loop. System identification. Prentice Hall, New York, pp 381–421
99. Kawada T, Sato T, Inagaki M, Shishido T, Tatewaki T, Yanagiya Y, Zheng C, Sugimachi M, Sunagawa K (2000) Closed-loop identification of carotid sinus baroreflex transfer characteristics using electrical stimulation. Jpn J Physiol 50:371–380
100. Harada S, Imaizumi T, Ando S, Hirooka Y, Sunagawa K, Takeshita A (1992) Arterial baroreflex dynamics in normotensive and spontaneously hypertensive rats. Am J Physiol 263:R524–R528
101. Masaki H, Imaizumi T, Harasawa Y, Takeshita A (1994) Dynamic arterial baroreflex in rabbits with heart failure induced by rapid pacing. Am J Physiol 267:H92–H99
102. Kawada T, Uemura K, Kashihara K, Kamiya A, Sugimachi M, Sunagawa K (2004) A derivative-sigmoidal model reproduces operating point-dependent baroreflex neural arc transfer characteristics. Am J Physiol Heart Circ Physiol 286:H2272–H2279
103. Ursino M, Fiorenzi A, Belardinelli E (1996) The role of pressure pulsatility in the carotid baroreflex control: a computer simulation study. Comput Biol Med 26:297–314
104. Uemura K, Sugimachi M, Kawada T, Kamiya A, Jin Y, Kashihara K, Sunagawa K (2004) A novel framework of circulatory equilibrium. Am J Physiol Heart Circ Physiol 286:H2376–H2385
105. Korenberg MJ, Hunter IW (1996) The identification of nonlinear biological systems: Volterra kernel approaches. Ann Biomed Eng 24:250–268
106. Moslehpour M, Kawada T, Sunagawa K, Sugimachi M, Mukkamala R (2015) Nonlinear identification of the total baroreflex arc. Am J Physiol Regul Integr Comp Physiol (**in press**)
107. Reid IA (1992) Interactions between ANG II, sympathetic nervous system, and baroreceptor reflexes in regulation of blood pressure. Am J Physiol 262:E763–E778
108. Kashihara K, Takahashi Y, Chatani K, Kawada T, Zheng C, Li M, Sugimachi M, Sunagawa K (2003) Intravenous angiotensin II does not affect dynamic baroreflex characteristics of the neural or peripheral arc. Jpn J Physiol 53:135–143
109. Kawada T, Shimizu S, Kamiya A, Sata Y, Uemura K, Sugimachi M (2011) Dynamic characteristics of baroreflex neural arc and peripheral arcs are preserved in spontaneously hypertensive rats. Am J Physiol Regul Integr Comp Physiol 300:R155–R165
110. Liu JL, Zucker IH (1999) Regulation of sympathetic nerve activity in heart failure: a role for nitric oxide and angiotensin II. Circ Res 84:417–423
111. Gao L, Schultz HD, Patel KP, Zucker IH, Wang W (2005) Augmented input from cardiac sympathetic afferents inhibits baroreflex in rats with heart failure. Hypertension 45:1173–1181
112. Huang C, Yoshimoto M, Miki K, Johns EJ (2006) The contribution of brain angiotensin II to the baroreflex regulation of renal sympathetic nerve activity in conscious normotensive and hypertensive rats. J Physiol 574:597–604
113. Kishi T (2013) Regulation of the sympathetic nervous system by nitric oxide and oxidative stress in the rostral ventrolateral medulla: 2012 Academic Conference Award from the Japanese Society of Hypertension. Hypertens Res 36:845–851
114. Miyano H, Kawada T, Shishido T, Sato T, Sugimachi M, Alexander J Jr, Sunagawa K (1997) Inhibition of NO synthesis minimally affects the dynamic baroreflex regulation of sympathetic nerve activity. Am J Physiol 272:H2446–H2452
115. Miyano H, Kawada T, Sugimachi M, Shishido T, Sato T, Alexander J Jr, Sunagawa K (1997) Inhibition of NO synthesis does not potentiate dynamic cardiovascular response to sympathetic nerve activity. Am J Physiol 273:H38–H43
116. Kamiya A, Kawada T, Yamamoto K, Michikami D, Ariumi H, Uemura K, Zheng C, Shimizu S, Aiba T, Miyamoto T, Sugimachi M, Sunagawa K (2005) Resetting of the arterial baroreflex increases orthostatic sympathetic activation and prevents postural hypotension in rabbits. J Physiol 566:237–246
117. Hajduczok G, Hade JS, Mark AL, Williams JL, Felder RB (1991) Central command increases sympathetic nerve activity during spontaneous locomotion in cats. Circ Res 69:66–75
118. Kamiya A, Kawada T, Yamamoto K, Mizuno M, Shimizu S, Sugimachi M (2008) Upright tilt resets dynamic transfer function of baroreflex neural arc to minify the pressure disturbance in total baroreflex control. J Physiol Sci 58:189–198
119. Abe C, Kawada T, Sugimachi M, Morita H (2011) Interaction between vestibulo-cardiovascular reflex and arterial baroreflex during postural change in rats. J Appl Physiol 111:1614–1621
120. Ray CA, Carter JR (2003) Vestibular activation of sympathetic nerve activity. Acta Physiol Scand 177:313–319
121. Gotoh TM, Fujiki N, Matsuda T, Gao S, Morita H (2004) Roles of baroreflex and vestibulosympathetic reflex in controlling arterial blood pressure during gravitational stress in conscious rats. Am J Physiol Regul Integr Comp Physiol 286:R25–R30
122. Verberne AJ, Guyenet PG (1992) Medullary pathway of the Bezold-Jarisch reflex in the rat. Am J Physiol 263:R1195–R1202
123. Kashihara K, Kawada T, Li M, Sugimachi M, Sunagawa K (2004) Bezold-Jarisch reflex blunts arterial baroreflex via the shift of neural arc toward lower sympathetic nerve activity. Jpn J Physiol 54:395–404
124. Kawada T, Yamazaki T, Akiyama T, Shishido T, Inagaki M, Uemura K, Miyamoto T, Sugimachi M, Takaki H, Sunagawa K (2001) In vivo assessment of acetylcholine-releasing function at cardiac vagal nerve terminals. Am J Physiol Heart Circ Physiol 281:H139–H145
125. Kashihara K, Kawada T, Yanagiya Y, Uemura K, Inagaki M, Takaki H, Sugimachi M, Sunagawa K (2003) Bezold-Jarisch reflex attenuates dynamic gain of baroreflex neural arc. Am J Physiol Heart Circ Physiol 285:H833–H840
126. Brodie TG (1900) On reflex cardiac inhibition. J Physiol 26:92–106
127. Löffelholz K, Muscholl E (1970) Inhibition by parasympathetic nerve stimulation of the release of the adrenergic transmitter. Naunyn Schmiedebergs Arch Pharmakol 267:181–184
128. Muscholl E (1980) Peripheral muscarinic control of norepinephrine release in the cardiovascular system. Am J Physiol 239:H713–H720
129. Levy MN (1971) Sympathetic-parasympathetic interactions in the heart. Circ Res 29:437–445
130. Klabunde RE (2012) Neurohumoral control of the heart and circulation. In: Cardiovascular physiology concepts, 2nd edn. Lippincott Williams and Wilkins. Philadelphia, pp 124–147
131. Matsuura W, Sugimachi M, Kawada T, Sato T, Shishido T, Miyano H, Nakahara T, Ikeda Y, Alexander J Jr, Sunagawa K (1997) Vagal stimulation decreases left ventricular contractility mainly through negative chronotropic effect. Am J Physiol 273:H534–H539
132. Nakayama Y, Miyano H, Shishido T, Inagaki M, Kawada T, Sugimachi M, Sunagawa K (2001) Heart rate-independent vagal effect on end-systolic elastance of the canine left ventricle under various levels of sympathetic tone. Circulation 104:2277–2279
133. Kawada T, Yamazaki T, Akiyama T, Li M, Ariumi H, Mori H, Sunagawa K, Sugimachi M (2006) Vagal stimulation suppresses ischemia-induced myocardial interstitial norepinephrine release. Life Sci 78:882–887

134. Shimizu S, Akiyama T, Kawada T, Shishido T, Yamazaki T, Kamiya A, Mizuno M, Sano S, Sugimachi M (2009) In vivo direct monitoring of vagal acetylcholine release to the sinoatrial node. Auton Neurosci 148:44–49
135. Kawada T, Akiyama T, Shimizu S, Kamiya A, Uemura K, Sata Y, Shirai M, Sugimachi M (2012) Central vagal activation by alpha$_2$-adrenergic stimulation is impaired in spontaneously hypertensive rats. Acta Physiol 206:72–79
136. Yamamoto H, Kawada T, Kamiya A, Kita T, Sugimachi M (2008) Electroacupuncture changes the relationship between cardiac and renal sympathetic nerve activities in anesthetized cats. Auton Neurosci 144:43–49
137. Uchida S, Kagitani F, Hotta H (2010) Neural mechanisms of reflex inhibition of heart rate elicited by acupuncture-like stimulation in anesthetized rats. Auton Neurosci 157:18–23
138. Li P, Pitsillides KF, Rendig SV, Pan HL, Longhurst JC (1998) Reversal of reflex-induced myocardial ischemia by median nerve stimulation: a feline model of electroacupuncture. Circulation 97:1186–1194
139. Ma L, Cui B, Shao Y, Ni B, Zhang W, Luo Y, Zhang S (2014) Electroacupuncture improves cardiac function and remodeling by inhibition of sympathoexcitation in chronic heart failure rats. Am J Physiol Heart Circ Physiol 306:H1464–H1471
140. Kawada T, Shimizu S, Yamamoto H, Shishido T, Kamiya A, Miyamoto T, Sunagawa K, Sugimachi M (2009) Servo-controlled hind-limb electrical stimulation for short-term arterial pressure control. Circ J 73:851–859
141. Meredith PA, Elliott HL (2004) Dihydropyridine calcium channel blockers: basic pharmacological similarities but fundamental therapeutic differences. J Hypertens 22:1641–1648
142. Yamamoto H, Kawada T, Shimizu S, Kamiya A, Miyazaki S, Sugimachi M (2013) Effects of cilnidipine on sympathetic outflow and sympathetic arterial pressure and heart rate regulations in rats. Life Sci 92:1202–1207
143. Yamamoto H, Kawada T, Shimizu S, Kamiya A, Turner MJ, Miyazaki S, Sugimachi M (2015) Acute effects of intravenous nifedipine and azelnidipine on open-loop baroreflex static characteristics in rats. Life Sci 126:37–41
144. Yamazaki T, Akiyama T, Kitagawa H, Takauchi Y, Kawada T, Sunagawa K (1997) A new, concise dialysis approach to assessment of cardiac sympathetic nerve terminal abnormalities. Am J Physiol 272:H1182–H1187
145. Kawada T, Yamamoto H, Shimizu S, Turner MJ, Sugimachi M (2013) Effects of L-type Ca^{2+} channel blocker nifedipine on dynamic arterial blood pressure control. Conf Proc IEEE Eng Med Biol Soc 2013:3805–3808
146. Dibner-Dunlap ME, Thames MD (1992) Control of sympathetic nerve activity by vagal mechanoreflexes is blunted in heart failure. Circulation 86:1929–1934
147. Feng Q, Sun X, Lu X, Edvinsson L, Hedner T (1999) Decreased responsiveness of vascular postjunctional α_1-, α_2-adrenoceptors and neuropeptide Y1 receptors in rats with heart failure. Acta Physiol Scand 166:285–291
148. Li M, Zheng C, Sato T, Kawada T, Sugimachi M, Sunagawa K (2004) Vagal nerve stimulation markedly improves long-term survival after chronic heart failure in rats. Circulation 109:120–124
149. Kawada T, Li M, Zheng C, Shimizu S, Uemura K, Turner MJ, Yamamoto H, Sugimachi M (2014) Chronic vagal nerve stimulation improves baroreflex neural arc function in heart failure rats. J Appl Physiol 116:1308–1314
150. Zanchetti A, Mancia G (1991) Cardiovascular reflexes and hypertension. Hypertension 18:III13–III21
151. Sapru HN, Wang SC (1976) Modification of aortic baroreceptor resetting in the spontaneously hypertensive rat. Am J Physiol 230:664–674
152. Andresen MC, Krauhs JM, Brown AM (1978) Relationship of aortic wall and baroreceptor properties during development in normotensive and spontaneously hypertensive rats. Circ Res 43:728–738
153. Nosaka S (1972) Features of efferent and afferent components of neural vascular control system in the spontaneously hypertensive rat. Jpn Circ J 36:569–573
154. Shastri S, Gopalakrishnan V, Poduri R, Wang HD (2002) Tempol selectively attenuates angiotensin II evoked vasoconstrictor responses in spontaneously hypertensive rats. J Hypertens 20:1381–1391
155. Mills E, Bruckert JW (1988) Pressor mechanisms linked obligatory to spontaneous hypertension in the rat. Hypertension 11:427–432
156. Hirooka Y (2015) Importance of neural arc for baroreflex resetting in hypertension. Circ J 79:510–512
157. Kishi T, Hirooka Y, Kimura Y, Ito K, Shimokawa H, Takeshita A (2004) Increased reactive oxygen species in rostral ventrolateral medulla contribute to neural mechanisms of hypertension in stroke-prone spontaneously hypertensive rats. Circulation 109:2357–2362
158. Kawada T, Sata Y, Shimizu S, Turner MJ, Fukumitsu M, Sugimachi M (2015) Effects of tempol on baroreflex neural arc versus peripheral arc in normotensive and spontaneously hypertensive rats. Am J Physiol Regul Integr Comp Physiol 308:R957–R964
159. Turner MJ, Kawada T, Shimizu S, Fukumitsu M, Sugimachi M (2015) Differences in the dynamic baroreflex characteristics of unmyelinated and myelinated central pathways are less evident in spontaneously hypertensive rats. Am J Physiol Regul Integr Comp Physiol (**in press**)
160. Abe C, Nagai Y, Yamaguchi A, Aoki H, Shimizu S, Akiyama T, Kawada T, Sugimachi M, Morita H (2015) Reduced carotid baroreceptor distensibility-induced baroreflex resetting contributes to impairment of sodium regulation in rats fed a high-fat diet. Am J Physiol Heart Circ Physiol 308:H942–H950
161. Cowley AW Jr, Liard JF, Guyton AC (1973) Role of baroreceptor reflex in daily control of arterial blood pressure and other variables in dogs. Circ Res 32:564–576
162. Chapleau MW, Hajduczok G, Abboud FM (1989) Peripheral and central mechanisms of baroreflex resetting. Clin Exp Pharmacol Physiol Suppl 15:31–43
163. Thrasher TN (2002) Unloading arterial baroreceptors causes neurogenic hypertension. Am J Physiol Regul Integr Comp Physiol 282:R1044–R1053
164. Lohmeier TE, Iliescu R, Dwyer TM, Irwin ED, Cates AW, Rossing MA (2010) Sustained suppression of sympathetic activity and arterial pressure during chronic activation of the carotid baroreflex. Am J Physiol Heart Circ Physiol 299:H402–H409
165. Braunwald E, Epstein SE, Glick G, Wechsler AS, Braunwald NS (1967) Relief of angina pectoris by electrical stimulation of the carotid-sinus nerves. N Engl J Med 277:1278–1283
166. Epstein SE, Beiser GD, Goldstein RE, Stampfer M, Wechsler AS, Glick G, Braunwald E (1969) Circulatory effects of electrical stimulation of the carotid sinus nerves in man. Circulation 40:269–276
167. Alnima T, Goedhart EJ, Seelen R, van der Grinten CP, de Leeuw PW, Kroon AA (2015) Baroreflex activation therapy lowers arterial pressure without apparent stimulation of the carotid bodies. Hypertension 65:1217–1222
168. Zucker IH, Hackley JF, Cornish KG, Hiser BA, Anderson NR, Kieval R, Irwin ED, Serdar DJ, Peuler JD, Rossing MA (2007) Chronic baroreceptor activation enhances survival in dogs with pacing-induced heart failure. Hypertension 50:904–910

169. Sabbah HN, Gupta RC, Imai M, Irwin ED, Rastogi S, Rossing MA, Kieval RS (2011) Chronic electrical stimulation of the carotid sinus baroreflex improves left ventricular function and promotes reversal of ventricular remodeling in dogs with advanced heart failure. Circ Heart Fail 4:65–70
170. Gronda E, Seravalle G, Trevano FQ, Costantino G, Casini A, Alsheraei A, Lovett EG, Vanoli E, Mancia G, Grassi G (2015) Long-term chronic baroreflex activation: persistent efficacy in patients with heart failure and reduced ejection fraction. J Hypertens 33:1704–1708
171. Kawada T, Yamazaki T, Akiyama T, Shishido T, Miyano H, Sato T, Sugimachi M, Alexander J Jr, Sunagawa K (1997) Interstitial norepinephrine level by cardiac microdialysis correlates with ventricular contractility. Am J Physiol 273:H1107–H1112
172. Kawada T, Miyamoto T, Miyoshi Y, Yamaguchi S, Tanabe Y, Kamiya A, Shishido T, Sugimachi M (2006) Sympathetic neural regulation of heart rate is robust against high plasma catecholamines. J Physiol Sci 56:235–245